OSKARI KAUSIALA
SECONDARY ORGANIC AEROSOL FORMATION FROM POLY-CYCLIC AROMATIC PRECURSORS

Master of Science Thesis

TIIVISTELMÄ

Polysykliset aromaattiset hiilvedyt (PAH) ovat orgaanisia yhdisteitä, jotka emittoituvat ilmakehään pääasiassa fossiilisten polttoaineiden ja biomassan epätäydellisen palamisen seurauksena. PAHien elinkaaren ymmärtäminen erityisesti urbaanissa ilmakehässä on tärkeää niiden myrkyllisyyden sekä sekundääriaerosolin muodostuspotentiaalin vuoksi.

Tässä työssä tutkittiin rakenteeltaan yksinkertaisimman PAHin – naftaleenin – hapettumisreaktioita sekä uusien hiukkasten muodostuspotentiaalia. Kirjallisuuskatsaus tehtiin tunnettujen OH-reaktiomekanismien, ja kyvyn muodostaa sekundääristä orgaanista aerosolia, selvittämiseksi. Kaksi laboratoriokoetta suoritettiin aiheen tutkimiseksi.

Ensimmäisen kokeen tavoitteena oli karakterisoida kvalitatiivisesti osa reaktiotuotteista. Tämä tehtiin hapettamalla naftaleenia virtausputkessa, ja mittaamalla tuotteita kemiallisesti ionisoivalla massaspektrometrillä. Toisessa kokeessa suuri konsentraatio hapetustuotteita muodostettiin TSARissa, jota monitoroitiin sekä hiukkasmittareilla (PSM ja SMPS) että massaspektrometrillä.

Tulokset osoittavat, että naftaleenin OH-hapetuksessa syntyy nopeasti äärimmäisen matalahöyrynpaineisia orgaanisia yhdisteitä. Hapetustuotteet muuntuvat hiukkasfaasiin ja synnyttävät hiukkasia, jotka ovat kooltaan vain muutamia nanometrejä. Oligomeerisiä tuotteita havaittiin kaasufaasin massaspektrissä, ja niiden syntyyn todennäköisesti johtava reaktiopolku esitetään kirjallisuusselvitykseen perustuen.

ABSTRACT

Polycyclic aromatic hydrocarbons (PAHs) are organic compounds that are emitted into the atmosphere mainly through incomplete combustion of fossil fuels and biomass. The lifecycle of PAHs especially in urban atmosphere is of great interest due to their toxicity and secondary aerosol formation potential.

In this thesis, the oxidation reactions and new particle formation potential of the structurally simplest polycyclic aromatic hydrocarbon – naphthalene – were studied. Literature survey was made on the OH initiated oxidation reaction mechanisms of naphthalene, as well as its' ability to produce secondary organic aerosol. Two laboratory experiments were carried out in order to study the subject.

The aim of the first experiment was to qualitatively characterize some of the oxidation products. This was done by oxidizing naphthalene in a flow tube and measuring the products with a chemical ionization mass spectrometer. In the second experiment, a large concentration of the oxidation products was generated in TSAR, while being monitored with both particle instrumentation (PSM and SMPS) as well as a mass spectrometer.

The results show that extremely low-volatility organic compounds are formed rapidly in the OH initiated oxidation of naphthalene. The oxidation products readily transform into the particle phase to form particles in the size scale of just a few nanometers. Oligomeric species were observed in the mass spectrum, and the reaction pathway leading to their formation is suggested based on the existing literature.

ACKNOWLEDGEMENTS

CONTENTS

LIST OF FIGURES

LIST OF TABLES

LIST OF ABBREVIATIONS AND SYMBOLS

Abbreviations

CCN	cloud condensation nuclei
CI-API-TOF	chemical ionization atmospheric pressure interface time of flight mass spectrometer
ELVOC	extremely low volatility organic compound
GR	growth rate
LRT	long range transport
LVOC	low volatility
NAP	naphthalene
NPF	new particle formation
OA	organic aerosol
PA	primary aerosol
PAH	polycyclic aromatic hydrocarbon
PM	primary matter
POA	primary organic aerosol
PSM	particle size magnifier
SA	secondary aerosol
SMPS	scanning mobility particle sizer
SOA	secondary organic aerosol
SVOC	semi-volatile organic compounds
TSAR	TUT secondary aerosol reactor
U.S. EPA	United States Environmental Protection Agency
UV	ultra violet
VOC	volatile organic compounds

Latin letters

A_i	particle phase concentration of species i
C	concentration
C^*	saturation mass concentration
C^o	saturation concentration
C_v	condensing vapor concentration
D	dilution factor
G	mass concentration

k	Boltzmann constant, reaction rate coefficient
K	gas to particle partitioning coefficient
M_o	organic aerosol mass concentration
M_w	molecular weight
P	pressure
R	gas constant
T	temperature
p	partial pressure
p^o	saturation vapor pressure
Q	volumetric flow rate
t	time
$[X]$	concentration of species X

Greek letters

α_m	mass accomodation coefficient
χ	mole fraction
γ	activity coefficient
λ	wavelength
ρ_v	vapor condensed phase density

1. INTRODUCTION

The Earth's atmosphere is a highly complex system consisting of thousands of individual gas phase chemical species, as well as particulate matter spanning the size range from just a few nanometers up to about 100 micrometers in diameter. Composition of the atmosphere is in part determined by what happens on the Earth, but also affected by the sunlight which induces photochemical processes that chemically transform its constituents. As a result, the chemical compounds in the atmosphere may also transition between gas and particle phase.

The term *aerosol* is used to refer to a colloid of particles suspended in air – or some other gas – including both the particles and the gas. Aerosols greatly affect the climate, both directly by absorbing and scattering solar radiation, and indirectly by acting as seeds for cloud droplets (Kroll & Seinfeld 2008). In addition to climate effects, aerosols have been shown to have an important impact on human health. They have been estimated to be the cause of more than two million premature, respiratory and cardiopulmonary system related deaths annually (Silva et al. 2013).

The lifespan of a particle in the atmosphere has been subject to extensive studies for over a century already, and the processes governing their birth and growth have revealed to be complex. Modern measurement technology has provided means to characterize molecules in gas phase, that are able to form new particles by colliding with each other, as well as to measure the number size distribution of these newly formed particles – just a few nanometers in size.

In this thesis, the particle formation potential of a polycyclic aromatic hydrocarbon, *naphthalene*, is studied. The work consists of theoretical and experimental parts. The theoretical part begins with discussion about the characteristics and role of aerosols in the atmosphere. Particle formation and in relation, polycyclic aromatic hydrocarbons are discussed – finally narrowing down to naphthalene. The currently known reaction mechanisms in the hydroxyl radical initiated oxidation of naphthalene are shown. In the experimental part, a chemical ionization mass spectrometer is used to study the oxidation products of naphthalene. New particle formation events from these precursors are studied in an oxidation flow reactor experiment.

2. ATMOSPHERIC AEROSOLS

Atmospheric aerosols consist of liquid or solid particles suspended in air – the term aerosol referring to both the particles and the gas. There is a large variety of globally important sources emitting aerosols into the atmosphere. Typical examples of natural sources would be oceans, deserts, forests and forest fires, volcanoes and all living organisms throughout their lives – while anthropogenic sources include practically all kinds of industry, and predominantly all human action where the combustion process is involved. Considering the variety of aerosol sources, it should be clear that the atmosphere is a complex mixture of vast amount of individual gas phase species in different concentrations, as well as widely varying number size distribution of particulate matter, with certain chemical composition and phase. Moreover, it is a highly dynamic system, where the aerosols evolve through many different processes throughout their lifetime. Most gaseous compounds undergo chemical reactions with other species in the atmosphere, typically with atmospheric oxidants. New particles may form from gaseous precursors by *nucleation*, but some may also evaporate back into the gas phase. Particles may grow in size by *coagulation* or *condensation*, and eventually – after growing large enough in size – they will deposit due to gravitation. Typical residence times of particles in the atmosphere vary from a few days to weeks. The diameters of aerosol particles span over four orders of magnitude, from a few nanometers up to around 100 micrometers, and the particle number concentration is significant everywhere in the atmosphere – whether urban or remote – and may sometimes be as high as 10^7-10^8 particles/cm^3. (Seinfeld & Pandis 2006)

The aerosols are often classified based on their source of origin. *Primary aerosol* (*PA*) is emitted directly from the source into the atmosphere, whereas *secondary aerosol* (*SA*) consists of particles formed *in situ* by gas-particle partitioning of the reaction products of volatile or semi-volatile gas phase species. Furthermore, these two classes can be divided into their *natural* and *anthropogenic* counterparts, where the natural fraction is emitted from sources in the nature and the anthropogenic fraction results from human action. Anthropogenic sources of primary aerosol include processes such as biomass burning, combustion of fossil fuels and traffic. Volcanic eruptions and wind-driven suspension of fine particulate matter (such as mineral

dust or sea salt) are important natural sources. (Seinfeld & Pandis 2006) A large fraction (around 50%) of the total sub-micron aerosol mass in the troposphere has been shown to consist of organic material (De Gouw & Jimenez (2009), Kanakidou et al. (2005)).

Aerosols are an important constituent of the atmosphere in terms of air quality and climate. The smallest aerosol particles – in the size range 1–100 nanometers – are able to penetrate deep into the lungs, and have been linked to severe short- and long-term negative health effects such as asthma, cardio-respiratory disease and lung cancer. They also have a great impact on the Earth's climate both directly by interacting with solar radiation, and indirectly by affecting cloud formation processes as well as through heterogenous chemical reactions between particle and gas phase species. (De Gouw & Jimenez (2009), Kroll & Seinfeld (2008)) Despite the progress that has been made in the field during last decades, there is still a lot of uncertainty involved concerning the sources, composition, properties and mechanisms of formation of atmospheric aerosols (Hallquist et al. 2009).

2.1 Aerosols and human health

Aerosols have been shown to have an adverse impact on human health. In recent years, a connection between exposure to elevated levels of ambient aerosols and damage in the human respiratory and cardiovascular systems has been well established. During the last decades, a substantial amount of research has been done that has added to the evidence that breathing combustion-related fine *particulate matter* (*PM*) is harmful to human health. Both short- and long-term exposure to elevated PM levels have been linked to increased risk of cardiovascular disease and mortality, long-term repeated exposures showing larger and more persistent cumulative effects. (Shiraiwa et al. 2017)

Estimations of the PM health effects' response to concentration show near linear relationship, with no evidence of safe threshold levels. Various biological mechanisms by which PM exposure affects the health have been proposed, and most likely the observed health issue is an interlinked combination of different mechanistic pathways (Pope & Dockery 2006). Epidemiological studies typically refer to PM mass concentrations, but the composition of the aerosol is also important, as some health effects may be related to specific constituents – such as bioaerosols, PAHs and transition metals (Shiraiwa et al. 2017).

Poor air quality is said to be the largest environmental health risk (Shiraiwa et al. 2017). At the same time, the absence of clearly defined safe level of exposure poses a

challenge for regulators in setting meaningful air quality standards (Pope & Dockery 2006).

Despite the well recognized issue, there are still important open questions regarding PM pollution and human health. These include the identification of groups with elevated risk of getting sick, the impacts of PM exposure on infants and birth defects, the effect of ambient PM on risk of lung cancer and the role of various constituents of PM and their relative importance. (Pope & Dockery 2006)

2.2 Aerosols and climate

Basically all the energy that reaches the Earth comes from the Sun. The energy balance of the planet is therefore governed by the absorption and reflection of incoming solar radiation, and the infrared radiation of energy back to space. *Radiative forcing* is defined as the difference between the incoming and outgoing radiative energy, quantified at the top of the atmosphere (*tropopause*) in units of W/m^2 at Earth's surface. Incoming energy exceeding the outgoing energy would mean positive forcing and increasing temperature of the planet. Negative forcing, by the same logic, would lead to it cooling down. The most important factor in determining the radiative forcing of Earth is the atmosphere, where individual components may have positive or negative contribution to the net forcing. For example, greenhouse gases absorb some of the outgoing infrared radiation, preventing its escape to space, thereby having positive forcing and warming effect. On the other side, clouds reflect part of the incoming sunlight back to space before reaching the Earth, thus having negative forcing and cooling effect. Atmospheric aerosols, in turn, may have either positive or negative forcing depending on their optical properties. They also have a crucial role in many of the key atmospheric processes, for example by acting as cloud condensation nuclei, thus having both direct and indirect effects on the radiative forcing and climate. (Seinfeld & Pandis 2006)

Aerosol particles are essential to cloud formation in the atmosphere, as they act as seeds onto which *supersaturated* water vapor, where relative humidity exceeds 100%, can condense on. Particles with sufficient size to become activated to grow to fog or cloud droplets are termed *cloud condensation nuclei* (*CCN*). The minimum size for activation is dependent on the degree of supersaturation, but is typically in the range 50–150 nm. Once activated, CCN will spontaneously grow by condensation to form a water droplet with diameter of 10 μm or more. An average CCN will experience 5–10 cloud activation/evaporation cycles before being removed from the atmosphere in precipitation. (Seinfeld & Pandis 2006)

The number concentration as well as other properties, such as the chemical composition, of CCN will in part be governing the cloud formation process and its properties. In polluted areas, where the CCN number concentration is high, the resulting cloud will consist of smaller droplets than it would in clean atmosphere. This may have an effect on the cloud's *albedo*, i.e. its ability to scatter solar radiation, as well as on the onset of precipitation. Therefore to understand the indirect climate effects of aerosols, it is crucial to understand their formation and evolution processes in the atmosphere in detail. (Fuzzi et al. 2015)

Dry particles also scatter and absorb radiation, this is the direct climate effect of aerosol particles. Black carbon particles released mainly from combustion of fossil fuels and biomass have been estimated to be the second most important cause of global warming, after CO_2, in terms of direct effect on the radiative forcing (Jacobson 2001). Still, anthropogenic contribution to the total aerosol loading of the atmosphere has been estimated to have a net cooling effect on the climate, by having both, net negative direct forcing as well as negative indirect forcing by cloud adjustments due to aerosols. The confidence level on the estimate for indirect effects, however, is low. The positive forcing of black carbon is compensated for by other aerosols, such as *organic aerosol* (*OA*), which conversely is believed to have negative effect on the radiative forcing. (Stocker et al. 2013)
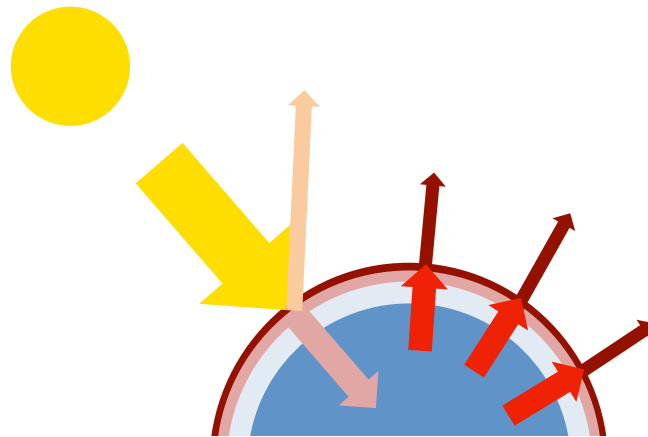
Figure 2.1 *Energy balance of the Earth is controlled by radiative forcing. Part of the incoming sun light is scattered back to space before reaching the surface, while another part is absorbed in the atmosphere. The rest hits the planet where the same process happens again. The Earth itself radiates heat at infrared wavelengths, part of which is absorbed in the atmosphere by greenhouse gases, the rest escaping to space.*

While much is known about the chemistry and physics of aerosols, as well as their effects on the climate, the complexity of the atmosphere poses a great challenge in putting all the pieces together in a meaningful way. A lot of work is yet to be done to

achieve a good understanding of the system and its evolution. One of the intriguing topics in the field of atmospheric science is *secondary organic aerosol* formation, where quantitative and predictive understanding is still lacking despite the progress made during recent years (Hallquist et al. 2009). Secondary aerosol is formed from organic or inorganic precursor gases reacting with atmospheric oxidants, forming products with lower volatility, which further partition into the particle phase by condensation or nucleation.

2.3   Secondary organic aerosol formation

Secondary organic aerosol (*SOA*) is formed in the atmosphere by the mass transfer of low-volatility oxidation products of *volatile organic compounds* (*VOC*) into the particle phase. VOCs are emitted into the atmosphere through the growth, maintenance and decay processes of plants, animals and microbes. Anthropogenic emissions arise mainly from the combustion of fossil fuels and biomass burning. It has been estimated that 10 000–100 000 individual organic species have been identified from the atmosphere, and that this may only represent a small fraction of all the species present (Goldstein et al. 2008). As VOCs are released into the atmosphere, they enter a complex system where they underg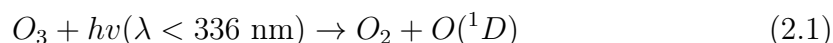o chemical transformation mainly by oxidizing agents such as the *hydroxyl radical* (OH), *ozone* (O_3) and the *nitrate radical* (NO_3), of which the OH radical is the most important one during daytime. It is also the primary oxidant in the atmospheric oxidation of *aromatic hydrocarbons*. (Atkinson et al. 2003)

The hydroxyl radicals are produced photochemically in the atmosphere, and therefore their concentration exhibits strong diurnal variation. The formation mechanism is a reaction cycle where first the photolysis of O_3 by short wavelength radiation produces an excited oxygen atom $O(^1D)$, as shown in equation 2.1. The excited oxygen can then react with a water molecule (H_2O) to produce two OH radicals (equation 2.2), or settle at the ground state ($O(^3P)$) by collisions with inert air molecules (M), such as N_2 (equation 2.3). Ground state atomic oxygen can react with molecular oxygen (O_2) to produce O_3 (equation 2.4), completing the cycle.

$$O_3 + hv(\lambda < 336 \text{ nm}) \rightarrow O_2 + O(^1D) \tag{2.1}$$

$$O(^1D) + H_2O \rightarrow 2OH \tag{2.2}$$

$$O(^1D) + M \rightarrow O(^3P) + M \tag{2.3}$$

$$O(^3P) + O_2 \rightarrow O_3 \tag{2.4}$$

The formation of other oxidants are not discussed in detail because they are not relevant in the scope of this thesis. Reactions between organic compounds and the oxidants may result in products with oxygen and possibly nitrogen containing functional groups, such as carboxylic acid (–C(O)OH), alcohol (–OH), ketone (=O) and nitro (–NO$_2$) groups. These products can have several orders of magnitude lower *saturation vapor pressure* than the parent molecule. Conversely, it is possible that a carbon–carbon bond will break in the reaction, leading to fragmentation and two higher volatility products. Ultimately, all the VOCs are oxidized up to CO or CO$_2$, if not deposited before that. Well known high yielding SOA precursors include *monoterpenes* (e.g. α-pinene), *sesquiterpenes* (e.g. β-caryophyllene) and to some extent aromatics (e.g. toluene). (Seinfeld & Pandis 2006)
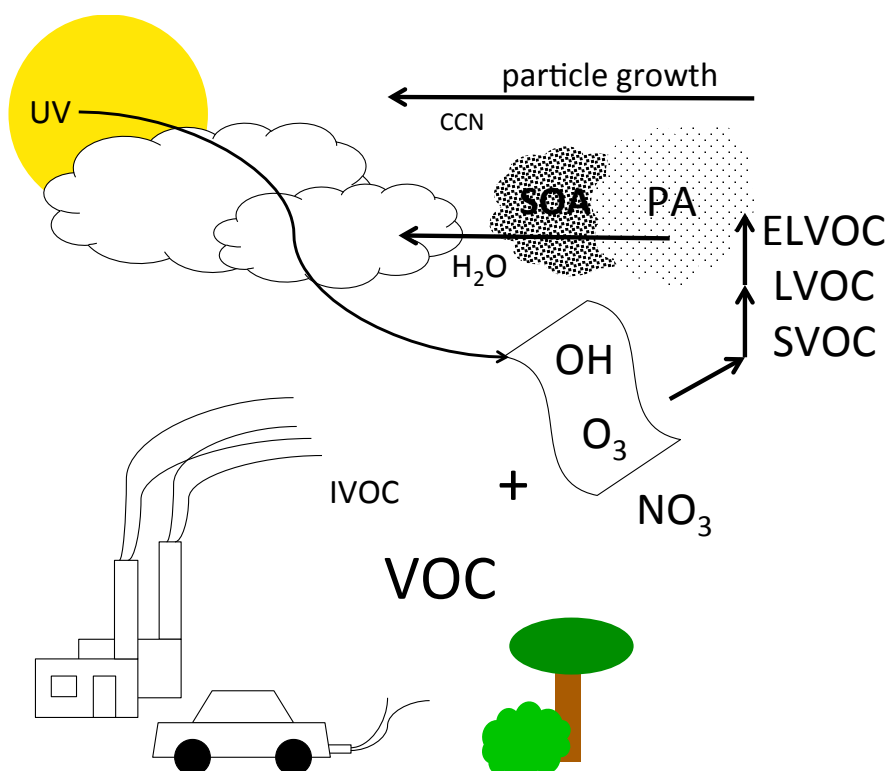
Figure **2.2** *Secondary organic aerosol formation process. VOCs emitted from various sources get oxidized by OH and O$_3$ generated by UV radiation, or NO$_3$. Reaction products are semi-volatile, low-volatility and possibly even extremely low-volatility organic compounds (SVOCs, LVOCs, ELVOCs) which condense on primary aerosol (PA), emitted by the same or some other source. The resulting SOA particles grow large enough in size to act as cloud condensation nuclei (CCN), and water condenses on the CCN to form clouds.*

Saturation vapor pressure is a critical property of an organic compound in determining how it partitions between the gas and particle phases in an aerosol. In this work, the terms *saturation vapor pressure* and *volatility* are used interchangeably, essentially to express the strength of the intermolecular forces determining how likely it

is for a molecule to stay in the gas phase. When polar functional groups are added to the molecule, these forces become stronger and the volatility decreases. Fragmentation, reducing the length of the carbon skeleton of the organic molecule, has the opposite effect. Therefore, whether the oxidation proceeds by functionalization or fragmentation will determine the direction of change of the saturation vapor pressure. It can be useful to classify the oxidation products based on their volatility, since it is an important factor in determining their atmospheric behavior. Donahue et al. (2012) proposed a following set of classes, in the order of decreasing volatility:

- **Volatile organic compounds** (VOC, $C^* > 3 \times 10^6$ μg m^{-3}) are emitted from various sources into the atmosphere, where they remain in the gas phase and undergo chemical transformation.

- **Intermediate volatility organic compounds** (IVOC, $300 < C^* < 3 \times 10^6$ μg m^{-3}) have quite low saturation vapor pressure, but still reside almost exclusively in the gas phase under atmospheric conditions. They are emitted from combustion processes, and have been proposed to significantly contribute to ambient OA (Robinson et al. 2007).

- **Semi-volatile organic compounds** (SVOC, $0.3 < C^* < 300$ μg m^{-3}) typically have a mass fraction in both aerosol and gas phase. This aerosol-specific definition includes compounds with much lower saturation vapor pressure than more general definition of semi-volatility. SVOCs may be emitted directly from a combustion source or form as a result of chemical transformation of VOCs in the atmosphere.

- **Low-volatility organic compounds** (LVOC, $3 \times 10^{-4} < C^* < 0.3$ μg m^{-3}) are found predominantly in particle phase in the atmosphere. They are formed in the atmosphere by functionalization of VOCs and SVOCs.

- **Extremely low-volatility organic compounds** (ELVOC, $C^* < 3 \times 10^{-4}$ μg m^{-3}) are almost exclusively in particle phase under any atmospherically relevant conditions. They can still evaporate in a thermodenuder. ELVOCs have been shown to significantly contribute to the early steps of new particle formation (Ehn et al. 2014).

Saturation mass concentration, C^*, is used in the classification and defined as γC^o, where C^o is the saturation concentration of a vapor over pure (sub-cooled) liquid and γ is the activity coefficient in a mixture. Saturation mass concentration is equivalent to *saturation vapor pressure* and *volatility* in the context of this thesis. Since organic aerosol is typically a complex mixture consisting of thousands of individual organic

compounds (Hildemann et al. (1991), Goldstein et al. (2008)), the thermodynamics of mixtures are important when considering SOA formation (Pankow 1994). That is, whether the condensing species with the existing organic mixture will tend to form a single, homogeneous phase or phase separate (Donahue et al. 2011). Phase separation may sharply reduce the predicted mass of the less abundant phase (Bowman & Melton 2004), and allow distinct types of organic aerosol to remain externally mixed (Asa-Awuku et al. 2009). Single OA phase, in turn, favors the formation of a uniform internal mixture.

The mass transfer flux of the oxidation products to the particle phase is dependent on the difference between the gas-phase concentrations on the particle surface and the surrounding gas. The system will be driven towards equilibrium, where these concentrations are equal and the mass transfer flux be zero. The equilibrium concentration, however, depends not only on the volatility of the species, but also its ability to form solutions with the compounds already present in the particle, such as other organics or water. (Seinfeld & Pandis 2006)

The partitioning equilibrium of semi-volatile species i, between gas and particle phase, can be described by the vapor pressure relation

$$p_i = \chi_i \gamma_i p_i^o, \tag{2.5}$$

where p_i is the partial pressure of species i in the gas phase, χ_i is the mole fraction of species i in the particulate phase, γ_i is its activity coefficient in the mixture particle and p_i^o is the saturation vapor pressure of species i over pure liquid. Partial pressure of i can be converted to its mass concentration G_i by the ideal gas law

$$G_i = \frac{p_i M_{wi}}{RT}, \tag{2.6}$$

where M_{wi} is the molecular weight of the species, R is the gas constant and T is the temperature. The mean molecular weight of n compounds in an aerosol particle can be expressed as

$$\overline{M}_w = \sum_i^n \chi_i M_{wi}. \tag{2.7}$$

Let us now denote the particle phase concentration of species i by A_i so that the total organic aerosol mass concentration M_o is

$$M_o = \sum_i^n A_i. \tag{2.8}$$

By assuming that the organic species have similar molecular weights, one can write

$$\chi_i = \frac{A_i}{M_o},$$ (2.9)

and substituting equations 2.6 and 2.9 into 2.5 yields

$$\frac{A_i}{G_i M_o} = \frac{RT}{\overline{M}_w \gamma_i p_i^o}.$$ (2.10)

The left hand side of equation 2.10 is the ratio of particle to gas phase mass concentration of species i, including the total particle phase mass concentration. Thus, the right hand side can be defined as the equilibrium gas to particle partitioning coefficient K_i of species i,

$$K_i = \frac{RT}{\overline{M}_w \gamma_i p_i^o},$$ (2.11)

where the activity coefficient γ_i depends on the mole fractions of all the species in the mixture as well as its temperature, and also p_i^o is temperature dependent. At a particular temperature, K_i is essentially constant for a given organic mixture. An important implication of equation 2.11 is that a greater fraction of each product will partition to the particle phase as the total organic aerosol concentration increases (Calvert et al. 2002).

The traditional approach to estimating the global SOA production is combining estimations of VOC fluxes with laboratory data from oxidation experiments leading to SOA formation. A simple way to quantify the SOA formation potential of a specific precursor species in reaction with an oxidant is to determine the aerosol mass yield

$$Y = \frac{\Delta M_0}{\Delta VOC},$$ (2.12)

which is defined as the ratio of the change in aerosol mass ΔM_0 to the amount of reacted precursor, ΔVOC. It should be noted though, that as discussed earlier, the interactions between the condensing species and the existing aerosol are dependent on their chemical composition and concentration as well as the surrounding conditions. Thus a mass yield determined in a laboratory experiment may have limited generalizability to actual atmospheric particle formation events.

Indeed, in a recent review by Tsigaridis et al. (2014), the results from a number of global SOA production models with different methodologies were shown to have large variation, in the range $13 - 121$ Tg a^{-1}, 19 Tg a^{-1} being the median estimated source strength. Comparison between observations and models revealed a large underestimation of the total (both primary and secondary) organic aerosol present

in the atmosphere. At urban locations, the comparison indicates missing knowledge on the strength and seasonality of anthropogenic OA sources. Currently many of the models neglect the contribution of anthropogenic VOCs to urban SOA formation completely (Tsigaridis et al. 2014), even though a recent estimate of 13.5 Tg a^{-1} makes it a non-negligible SOA source in polluted regions (De Gouw & Jimenez 2009). The rapid growth of SOA in urban air may overwhelm the direct POA emissions within a few hours of photochemical processing (Volkamer et al. 2006).

As discussed in section 2.2, the organic aerosol load in the atmosphere is expected to significantly affect the radiative forcing of Earth, and therefore there is an urgent need to reach a consensus between models and an agreement with observations. This is a necessity in order to be able to constrain the impact of organic aerosols on the climate. The conclusion made by De Gouw & Jimenez (2009) suggests that urban SOA formation could be a much larger source of aerosol at northern midlatitudes than previously recognized. Further research on the subject is needed to achieve a better understanding of the sources and processes controlling the global OA budget.

2.4   New particle formation

In addition to primary particle emissions, another important factor determining the number concentration of atmospheric particles is *new particle formation* (*NPF*). As condensable gaseous molecules are produced by chemical transformation in the atmosphere, they may either condense onto the surface of pre-existing aerosol, or nucleate to form new particles. The relative importance of each of these mechanisms depends on the thermodynamic properties of the condensing molecules as well as their formation rate, and the amount of aerosol particles available for them to condense on. (McMurry & Friedlander 1979)

New particle formation events have been observed in numerous locations around the Earth, in conditions ranging from clean Arctic (and Antarctic) air to industrial plumes. The findings suggest that these events occur all over the planet. There are, however, substantial variations in intensities and spatial scales of atmospheric NPF. In mid-latitudes, typical particle *growth rates* (*GR*) are in the range 1–20 nm h^{-1}, whereas in the polar regions rates as low as 0.1 nm h^{-1} are observed. The *formation rate* of 3 nm particles in regional nucleation events lies typically in the range 0.01–1 particles cm^{-3}s^{-1} in the boundary layer. However, in coastal environments and industrial plumes, formation rates as high as 10^4–10^5 particles cm^{-3}s^{-1} have been reported. Depending on the location, new particle formation and subsequent growth can increase the CCN concentration by a factor of more than two, over the course of

one day. Therefore NPF events are expected to significantly affect cloud formation. (Kulmala et al. 2004)

Even though new particle formation has been identified as a significant source of particles in the atmosphere, the understanding of the phenomenon is not complete. Recent findings suggest that nucleation and subsequent particle growth are uncoupled under atmospheric conditions. Sulphuric acid (H_2SO_4) vapor has been associated with atmospheric nucleation, but the mechanism remains to be definitely identified. The observations made in the free troposphere are well explained with binary water–H_2SO_4 nucleation, whereas in the boundary layer a third component (such as ammonia or low-volatility organics) or completely different nucleation mechanism is needed. (Kulmala & Kerminen 2008)

Nieminen et al. (2010) have investigated the condensational growth rate of particles smaller than 10 nm, and smaller than 3 nm in particular. They have derived an analytical approximation connecting particle growth rate to condensing vapor concentration, as follows

$$C_v = \frac{2\rho_v d_v}{\alpha_m m_v \Delta t} \cdot \sqrt{\frac{\pi m_v}{8kT}} \cdot \left[\frac{2x_1 + 1}{x_1(x_1 + 1)} - \frac{2x_0 + 1}{x_0(x_0 + 1)} + 2\ln\left(\frac{x_1(x_0 + 1)}{x_0(x_1 + 1)}\right) \right], \quad (2.13)$$

where the substitutions $x_0 = d_v/d_{p,initial}$ and $x_1 = d_v/d_{p,final}$ have been made. In equation 2.13, C_v is the condensing vapor concentration and ρ_v its density in condensed phase, α_m is the mass accomodation coefficient, m_v is the mass of the vapor molecule and k is the Boltzmann constant. The equation provides a relationship between the vapor concentration and particle growth in time Δt and temperature T, where d refers to the diameter and subscripts v and p to vapor and particle, respectively.

2.5 Polycyclic Aromatic Hydrocarbons (PAHs)

Polycyclic aromatic hydrocarbons (PAH) are a class of organic compounds consisting of two or more fused aromatic rings. PAHs and their derivatives are produced by the incomplete combustion of organic material, and thus released into the atmosphere mainly due to anthropogenic activity – while forest fires and volcanic eruptions are the major biogenic emission sources (Ravindra et al. 2008). The major anthropogenic emission sources include biomass burning, coal and petroleum combustion and coke and metal production. While the emissions in developed countries have decreased in the past decades, as the efficiency of energy utilization has improved, the trend in developing countries is the opposite. (Zhang & Tao 2009) The ubiq-

uitous presence of PAHs in the environment is of major concern due to the well known carcinogenicity of a number of species in this group (Keyte et al. 2013). The health risks of human exposure to PAHs have been studied for some decades already, and it has become clear that PAHs and their atmospheric reaction products (e.g. *nitro-PAH, oxy-PAH*) have a significant contribution on the mutagenic activity of ambient atmospheres (IARC (1983), Atkinson & Arey (1994), Ravindra et al. (2001), Umbuzeiro et al. (2008)). Human exposure to PAHs has been linked with DNA adducts and mutations as well as reproductive defects (Gaspari et al. (2003), Perera et al. (2002)).

PAHs are generally emitted from sources into the atmosphere as a complex mixture of numerous compounds, and thus monitoring the concentrations of all individual species is generally not possible. For this reason, surrogate compounds have been selected to represent these mixtures, and are used to monitor and regulate air quality with respect to polycyclic aromatic hydrocarbons. In 1976, the United States Environmental Protection Agency (U.S. EPA) listed 16 *Priority Pollutant PAHs* as representatives of PAHs to regulate (Keith 2015). The legislation has had a great impact as a primary driver for development of analytical methods to detect PAHs, and also more generally in the environmental sciences in the past 40 years. As such, the list has been well established among environmental scientists, and thus beneficial as a practical standardized test set. (Andersson & Achten 2015) However, as the list is already 40 years old and even originally composed with mostly practical aspects in mind (Keith 2015), the need for an update has been brought up in the recent scientific discussion (Keith (2015), Andersson & Achten (2015), Wise et al. (2015)).

In a recent study by Chan et al. (2009) it was shown that polycyclic aromatic hydrocarbons may significantly contribute to the SOA formation in urban atmospheres. Lighter aromatics, such as *benzene* and *toluene*, have traditionally been thought to be the major anthropogenic SOA precursors (Kroll & Seinfeld 2008), but the study by Chan et al. (2009) suggests that PAHs may produce 3–5 times more SOA mass, based on their yield measurement combined with emission inventories by Schauer et al. (2001). They estimate PAHs to account for up to 54% of SOA formed from diesel exhaust and up to 80% from fireplace wood burning. Considering the uncertainties involved in anthropogenic SOA formation (see 2.3), polycyclic aromatic hydrocarbons, recognized as being a potentially large source of urban SOA mass, should be a target for further SOA formation studies. A better understanding is needed to evaluate their impact on climate in global scale, as well as locally, keeping in mind their well recognized toxicity. Current atmospheric models do not include SOA formation from gas-phase reactions of PAHs (Chan et al. 2009).

Other intriguing question about PAHs is their *long-range transport* (*LRT*). A number of studies have reported an unexpectedly high LRT potential of particle-bound PAHs. While the gas phase PAH concentrations in the Arctic are much lower compared to Europe, the particle-phase concentrations are only slightly less. Moreover, based on the current understanding of gas-particle partitioning and atmospheric degradation of certain PAHs, they should not undergo LRT at all – yet they are found in the Arctic at nearly the same concentrations as in Europe. (Zelenyuk et al. 2012) The chemical and physical processes influencing the transport from high emission areas to remote regions are still largely unknown (Friedman et al. 2014). Zelenyuk et al. (2012) proposed a mechanism where SOA particles forming in the presence of hydrophobic organics – such as PAHs – adsorb these compounds on the particle surface. As the particles keep growing by condensation and coagulation, the hydrophobic compounds get trapped inside the highly viscous SOA particles. The SOA matrix protects the embedded PAHs from atmospheric oxidation, as well as prevents them from evaporating. For this to happen, the gas phase PAHs need to be present during the SOA formation, because it is unlikely for molecules adsorbed onto the particle surface to penetrate inside. Furthermore, they observed a synergetic relationship between PAHs and SOA, where the presence of even a small amount of PAH inside the SOA decreases its evaporation rate and amplifies the atmospheric aging process, ensuring efficient LRT for both the PAH and the SOA. The results of Friedman et al. (2014), however, suggest a different mechanism. They conclude that trapping PAHs in black carbon particles instead of SOA leads to better agreement between measured and simulated PAH concentrations in remote regions, as well as their phase distributions. This is in part due to the fact that sources producing the greatest PAH emissions are typically also emitting black carbon. Even though there is still uncertainty in the mechanisms of long-range transport of PAHs, it is important to note that they do exist. Therefore PAH emissions cannot be considered only as a local problem near the emission source. Also the issue serves as an example of the need to understand the thermodynamics of mixtures when considering the mechanisms of SOA formation, as discussed in section 2.3.
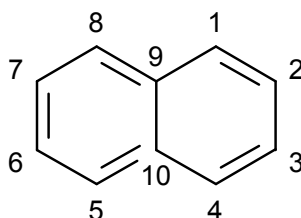

Figure 2.3 *Naphthalene molecular structure, consisting of two fused aromatic rings. Note the numbering of the carbon atoms.*

Naphthalene ($C_{10}H_8$) is a polycyclic aromatic hydrocarbon consisting of two fused aromatic rings, shown in figure 2.3. It is by molecular structure the simplest PAH. It is a major component of PAH emitted by diesel and gasoline powered motor vehicles (Schauer et al. (1999), Schauer et al. (2002)) and domestic wood combustion (Schauer et al. 2001). Reisen & Arey (2005) showed that naphthalene and alkyl-naphthalenes are the most abundant PAHs present in ambient air in Los Angeles. U.S. EPA has listed naphthalene as one of the 16 Priority Pollutant PAHs, and therefore it has also been studied extensively. Even so, much of the reaction mechanisms and consequently SOA formation mechanisms still remain unknown. Chan et al. (2009) determined the SOA yield of naphthalene and certain alkyl-naphthalenes in a photooxidation chamber study in the presence of an inorganic seed aerosol, and using the studied compounds as surrogates for PAHs, they would expect PAHs to significantly contribute to anthropogenic SOA formation. The yields they measured for naphthalene, as defined by equation 2.12, were approximately 0.2–0.3 under high-NO_x, and 0.6–0.7 under low-NO_x conditions. However, further study on the oxidation mechanisms and products of PAHs, as well as on the chemical composition of the formed SOA is needed. In the next chapter, the mechanisms of atmospheric oxidation of naphthalene are reviewed and discussed.

3. OH-INITIATED OXIDATION OF NAPHTHALENE

Main removal mechanism of naphthalene from the atmosphere is reaction with the hydroxyl radical (OH) (Bunce et al. 1997). Other potential removal pathway is the reaction with nitrate radical (NO_3), but it is outside the scope of this thesis. The mechanism of OH radical initiated oxidation of naphthalene has been studied for a few decades already (e.g. Atkinson et al. (1987), Bunce et al. (1997), Qu et al. (2006), Zhang et al. (2012)). Its structural simplicity allows quantum chemical computational study of the oxidation mechanism step by step – at least up to a point – and thus it serves as a good starting point for the research in PAH oxidation mechanisms in general. The currently proposed reaction mechanisms will be discussed next.

3.1 Initiation

The reaction between naphthalene and OH radical under atmospheric conditions takes place mainly *via* addition to position C_1 or C_2 (Shiroudi et al. (2014), Zhang et al. (2012), Qu et al. (2006), Ricca & Bauschlicher (2000)). Out of these, the addition to C_1 is more likely with branching ratio of approximately 90 %, whereas the addition to position C_2 occurs 10 % of the time, correspondingly (Shiroudi et al. (2014), Zhang et al. (2012)). The initiation step of the reaction sequence is presented in figure 3.1. The *alkyl radicals R1* and *R2* formed in the initiation are named after the carbon atom into which the OH addition takes place. Radicals are highly reactive, and therefore the reaction sequence proceeds promptly.

Lorenz & Zellner (1983) studied the temperature dependence of the reaction rate between naphthalene and the OH radical in the range 337–525 K, and discovered an inverse relationship at low temperatures. The reason for this is the decomposition reaction back to precursors, as denoted in figure 3.1 by the backwards reaction arrows. The decomposition has stronger temperature dependence compared to the addition reaction. At temperatures above 410 K the effective rate of OH addition drops significantly, and at even higher temperatures the dominant reaction mechanism shifts
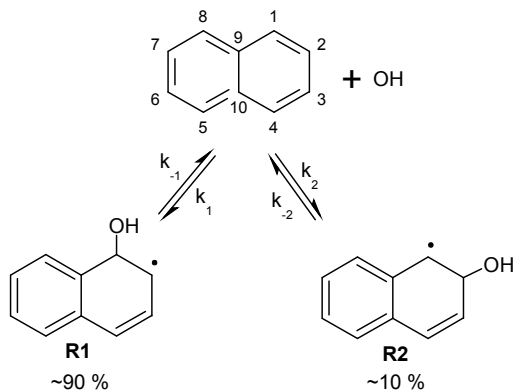
Figure 3.1 *The initiation reaction between naphthalene and the OH radical by addition. Approximately 90% of the time alkyl radical R1 is formed, while R2 accounts for the rest. Decomposition back to the reactants is possible and its rate increases with temperature.*

from OH addition to H abstraction (OH → H_2O). (Lorenz & Zellner 1983) In this work, however, the mechanism is studied at room temperature so only the OH addition pathway is considered significant. The temperature dependent reaction rate coefficient at temperatures (below 410 K) is given by

$$k_{NAP+OH} = (1.335 \pm 0.825) \times 10^{-12} e^{(902 \pm 240)/T} \text{ cm}^3 \text{ molecule}^{-1} \text{ s}^{-1} , \qquad (3.1)$$

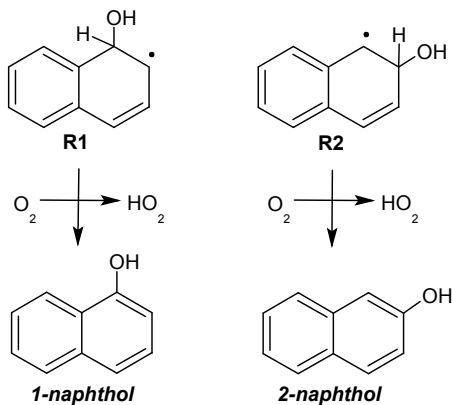where T is the temperature (Shiroudi et al. 2014).

Figure 3.2 *Hydrogen abstraction from radicals R1 and R2. The hydrogen atom bonded to the same carbon atom as the hydroxyl group (C_1 or C_2) may get abstracted by molecular oxygen, leading to the formation of a double bond between C_1 and C_2 and a closed shell product: 1-naphthol or 2-naphthol.*

After the initiation step, possible reaction pathways include hydrogen abstraction (O_2 → HO_2), O_2-addition and NO_2-addition (Zhang et al. (2012), Qu et al. (2006), Sasaki et al. (1997)) – in addition to the aforementioned decomposition (Qu et al.

(2006), Bunce et al. (1997), Lorenz & Zellner (1983)). Qu et al. (2006) determined in their computational study that energetically the most favorable (pseudo)-unimolecular reaction for *R1* and *R2* would be hydrogen abstraction, as shown in figure 3.2, leading to the formation of *1-naphtol* or *2-naphtol*, respectively. These compounds have also been identified as major oxidation products in experimental studies (Sasaki et al. (1997), Bunce et al. (1997)). According to Qu et al. (2006), other isomerization or decomposition reactions (except for the decomposition back to reactants) do not seem likely due to their high endotermicity. However, NO$_2$ and O$_2$ addition reactions were shown to be competitive with hydrogen abstraction. Under typical atmospheric conditions, O$_2$ addition would be the dominant reaction pathway. However, under high NO$_2$ concentrations (in a polluted atmosphere), the addition of NO$_2$ may also become significant. (Koch et al. (2007), Ghigo et al. (2006)) Let us first take a look into the details of the O$_2$ addition pathway.

3.2 O$_2$ addition

Radicals *R1* and *R2* have several resonance structures, and therefore the O$_2$ addition may take place into positions C$_2$, C$_4$, C$_5$, C$_7$ and C$_9$ in case of *R1*, and into C$_1$, C$_3$, C$_6$, C$_8$ and C$_{10}$ in case of *R2*. For *R1* the addition most likely occurs at positions C$_2$ or C$_4$, based on a quantum mechanical computation conducted by Zhang et al. (2012). The result seems intuitive, since addition to these positions leaves the other aromatic ring intact. Addition to position C$_2$ or C$_4$ will lead to the formation of a peroxy radical *R1-2OO* or *R1-4OO*, respectively, as shown in figure 3.3. Zhang et al. (2012) did not do the calculation for radical *R2*, but by assuming that conservation of the aromatic ring is favorable, the only available position for addition would be C$_1$, leading to the formation of a peroxy radical *R2-1OO*, as shown in figure 3.3.

Zhang et al. (2012) showed that the role of peroxy radical *R1-4OO* is of limited significance due to fast decomposition and slow propagation reactions. Qu et al. (2006) on the other hand made the conclusion in their study, that O$_2$ addition leads to either *R1-2OO* or *R2-1OO*, for *R1* and *R2* respectively. Thus, only these two pathways are considered further on and *R1-4OO* is ruled out as insignificant. Nishino et al. (2012) approximated the combined effective reaction rate constant of *R1* and *R2* with respect to O$_2$ addition to be in the order of $k_{O_2} \approx 1 \times 10^{-17}$ cm^3 molec^{-1} s^{-1}. The reaction chain propagates for peroxy radicals *R1-2OO* and *R2-1OO*, and is discussed in subsection 3.4.
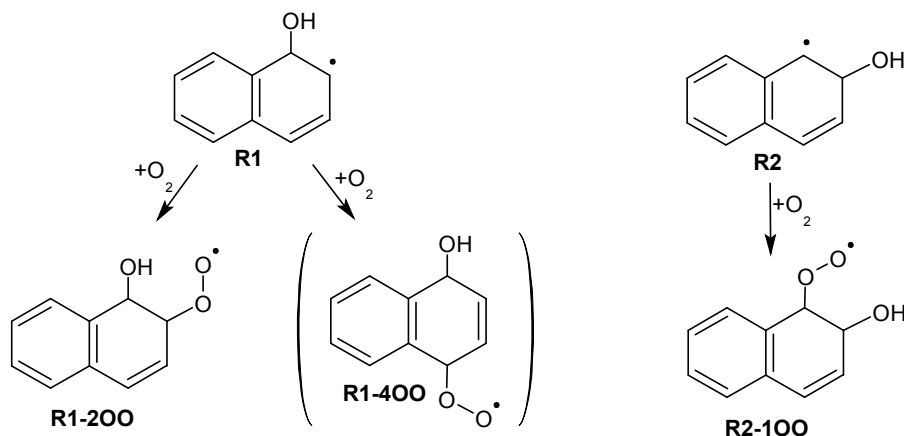
Figure 3.3 *O₂-addition to R1 and R2 leads to the formation of peroxy radicals R1-2OO or R1-4OO and R2-1OO, respectively. The role of R1-4OO is expected to be insignificant due to high decomposition and low propagation rates.*

3.3 NO₂ addition

Instead of O_2 addition, the reaction of radicals *R1* and *R2* may proceed with nitrogen dioxide (NO_2) addition. According to Ghigo et al. (2006), the branching ratio between O_2 and NO_2 addition is $\nu_{NO_2}/\nu_{O_2} \approx 10^{-5} - 10^{-1}$, when $[NO_2] = 0,004 - 40$ ppb. Nishino et al. (2008) determined $[NO_2] \approx 60$ ppb to be the concentration where $\nu_{NO_2}/\nu_{O_2} = 1$. In spite of being a minor reaction pathway under typical atmospheric conditions, the NO_2 addition is of special interest due to its potential to form nitro-group containing products (*nitro-PAHs*).

After the addition, the intermediate product may eliminate either a water (H_2O) or a nitrous acid (HONO) molecule, forming either *2-nitronaphthalene* or *1-naphthol* in reaction of *R1*, and *1-nitronaphthalene* or *2-naphthol* in reaction of *R2* (Sasaki et al. (1997), Atkinson et al. (1987)), as shown in figure 3.4. Qu et al. (2006) suggest H_2O elimination to be the main reaction channel. In contrast, Zhang et al. (2012) computed this channel to require crossing too high an energy barrier to be of any significance under atmospheric conditions. However, Kautzman et al. (2010), Sasaki et al. (1997) and Bunce et al. (1997) do report identifying experimentally both *2-nitronaphthalene* and *1-nitronaphthalene* as naphthalene oxidation products, and no other mechanism to explain their formation has been proposed.

Nishino et al. (2012) showed by experiment that the NO_2 addition pathway also leads to the formation of *2-formylcinnamaldehyde*, but the intermediate reaction steps are unknown. The NO_2 addition and following reactions for *R1* and *R2* are shown in figure 3.4. Nishino et al. (2012) approximated the combined reaction rate coefficient for both *R1* and *R2* with NO_2 to be $k_{NO_2} \approx 3 \times 10^{-11}$ cm³ molec⁻¹ s⁻¹.
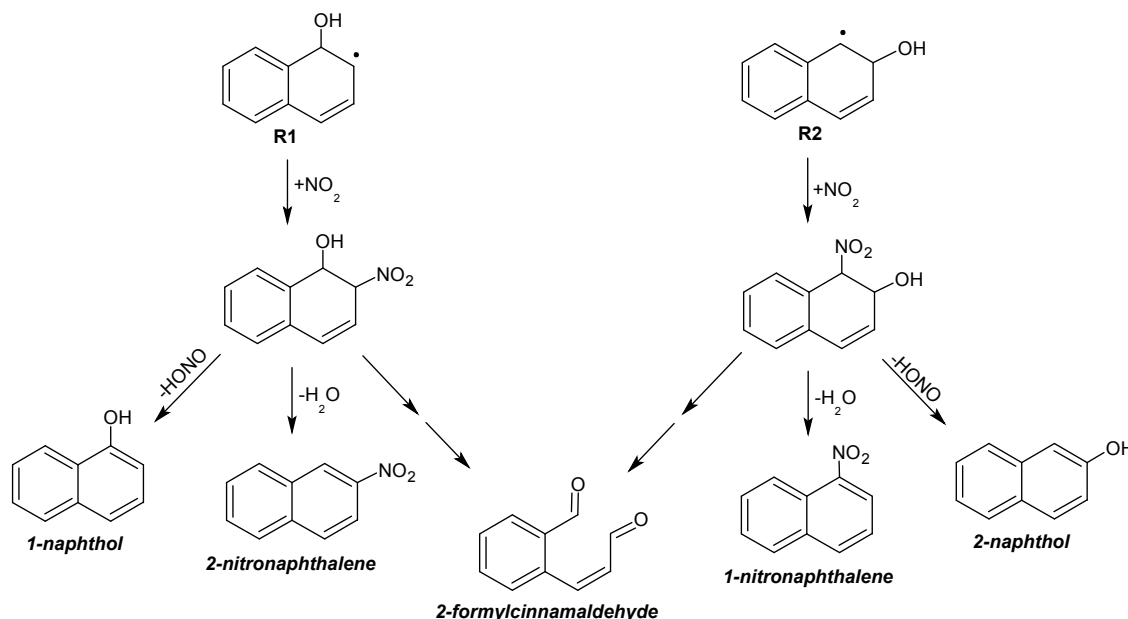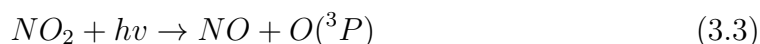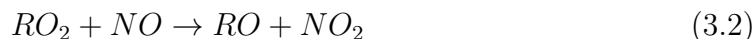
Figure 3.4 *NO_2-addition to R1 and R2, and subsequent reaction steps, lead to the formation of 1-naphthol or 2-nitronaphthalene from R1, and 2-naphthol or 1-nitronaphthalene from R2. Either of the precursor radicals may react to form 2-formylcinnamaldehyde, but the reaction steps remain unknown.*

3.4 Peroxy radical reactions

The initiation of a radical chain reaction by OH addition followed by a subsequent O_2 addition, leads to the formation of peroxy radicals – generally noted as RO_2 where R is an arbitrary hydrocarbon. Peroxy radicals in general play a central role in the chemistry of the troposphere. Most of the organic species present in the atmosphere form peroxy radicals in the initial steps of oxidation. The peroxy radicals may undergo bimolecular reactions with NO, NO_2, HO_2 or another peroxy radical $R'O_2$, or react unimolecularly. The propagation, and thus also the products, of the reaction depend on the atmospheric conditions and its chemical composition, as well as the amount of sunlight present. Typically the dominant reaction is that with nitrogen oxide (NO), especially in human habitated regions. As a result, the peroxy radical is converted into an alkoxy radical (RO) by reaction 3.2.

$$RO_2 + NO \rightarrow RO + NO_2 \tag{3.2}$$

$$NO_2 + hv \rightarrow NO + O(^3P) \tag{3.3}$$

$$O(^3P) + O_2 + M \rightarrow O_3 + M \tag{3.4}$$

The chain reaction for the formed alkoxy radical will continue. Reactions 3.2 and 3.3 are a part of the atmospheric NO_x-cycle. Considering reactions 3.2, 3.3 and 3.4, it is worth noticing that in urban areas where NO is always present, introducing RO_2 into the atmosphere will lead to O_3 formation, which is toxic to humans.
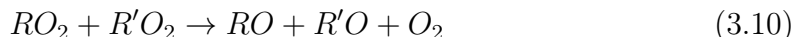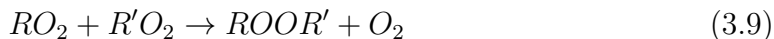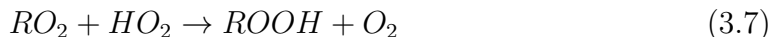
Competing, though usually much slower, reaction for 3.2 is the addition reaction 3.5 which leads to the formation of an organonitrate.

$$RO_2 + NO \rightarrow RONO_2 \tag{3.5}$$

A reaction 3.6 between RO_2 and NO_2 is also possible, but the peroxynitrates formed in the reaction are thermally unstable and thus it has significance only in very cold regions or in the upper atmosphere.

$$RO_2 + NO_2 + M \leftrightarrow RO_2NO_2 + M \tag{3.6}$$
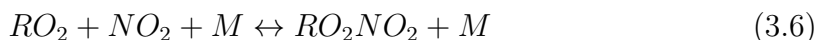
Instead, more significant reaction pathways are reactions with HO_2 and other peroxy radicals: reactions 3.7, 3.8, 3.9 and 3.10.

$$RO_2 + HO_2 \rightarrow ROOH + O_2 \tag{3.7}$$

$$RO_2 + R'O_2 \rightarrow ROH + R''CHO + O_2 \tag{3.8}$$

$$RO_2 + R'O_2 \rightarrow ROOR' + O_2 \tag{3.9}$$

$$RO_2 + R'O_2 \rightarrow RO + R'O + O_2 \tag{3.10}$$

In reaction 3.7 between the peroxy radical and a hydroperoxyl, an organic hydroperoxide is formed. Reactions between two (same or different) peroxy radicals may result in the formation of an alcohol and either an aldehyde or a ketone (reaction 3.8), or a dimer structure with an oxygen bridge between the two radicals (reaction 3.9). Reactions 3.7, 3.8 and 3.9 terminate the chain reaction, while 3.10 forms two alkoxy radicals which react further on. The branching ratio between reaction with NO (reaction 3.2) and other radicals (reactions 3.7, 3.8, 3.9 and 3.10) is an essential factor considering the ozone formation in lower atmosphere. (Orlando & Tyndall 2012)

In addition to the bimolecular reactions presented above, also unimolecular decomposition and isomerization reactions are possible especially for aromatic peroxy radicals (Glowacki & Pilling 2010). For benzene, HO_2 abstraction and cyclization have been shown to be significant reaction pathways for NO_x concentrations up to ~100 ppb (Bloss et al. 2005).

Now let us consider the peroxy radicals *R1-2OO* and *R2-1OO* formed after initiation of naphthalene oxidation (see section 3.2). Zhang et al. (2012) calculated unimolecular reaction rates for the radical *R1-2OO*, and comparing those with typical reaction rates between RO_2 and NO in the atmosphere (~1 s^{-1}, when [NO] ~4 ppb (Miller et al. 2004)) gives information about the relative importance of different reactions. The fastest unimolecular reaction for *R1-2OO* is a H-shift between the –OH and –OO· functional groups, and leads to the formation of an intermediate product *R1-P2O1*, which after a prompt OH elimination breaks the C_1–C_2 bond forming a *2-formylcinnamaldehyde* product (figure 3.5). Similar reaction sequence is possible for the radical *R2-1OO*, as shown in figure 3.6 (Qu et al. 2006).
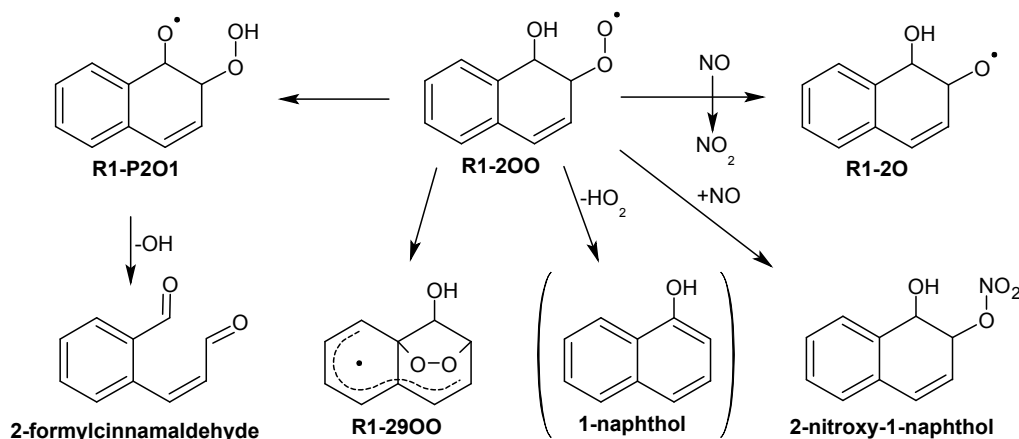

Figure 3.5 *The reaction sequence of peroxy radical R1-2OO under atmospheric conditions proceeds either unimolecularly, or with NO. Possible closed shell reaction products are 2-formylcinnamaldehyde, 2-nitroxy-1-naphthol and possibly 1-naphthol (see text). Intermediate radical products include alkyl radicals R1-29OO and R1-2O.*

In earlier research, the peroxide group (–OO·) of *R1-2OO* has been assumed to be able to form an oxygen bridge between C_2 and C_4, resulting in a bicyclic radical (Kautzman et al. (2010), Bunce et al. (1997)) similar to benzene oxidation. However, a more recent study by Zhang et al. (2012) suggests that cyclization is energetically unfavored, compared to other competing reactions. The only bridge forming reaction possible under atmospheric conditions would be an OO-bridge between C_2 and C_9 carbon atoms, forming *R1-29OO*, and thus possible only for *R1-2OO*. The rate of this reaction is in the order of ~10^{-2} s^{-1}, while other bridge forming reactions are too slow to have any significance (10^{-5}–10^{-15} s^{-1}) (Zhang et al. 2012). Qu et al. (2006) suggest an alternative decomposition pathway for *R1-2OO* and *R2-1OO*, where HO_2 radical is abstracted giving *1-naphthol* or *2-naphthol* product. A study by Hyttinen et al. (2016), however, suggests that HO_2 abstractions from organic peroxy radicals in general is unlikely under atmospheric conditions due to their slowness ($\leq 10^{-3}$ s^{-1}).
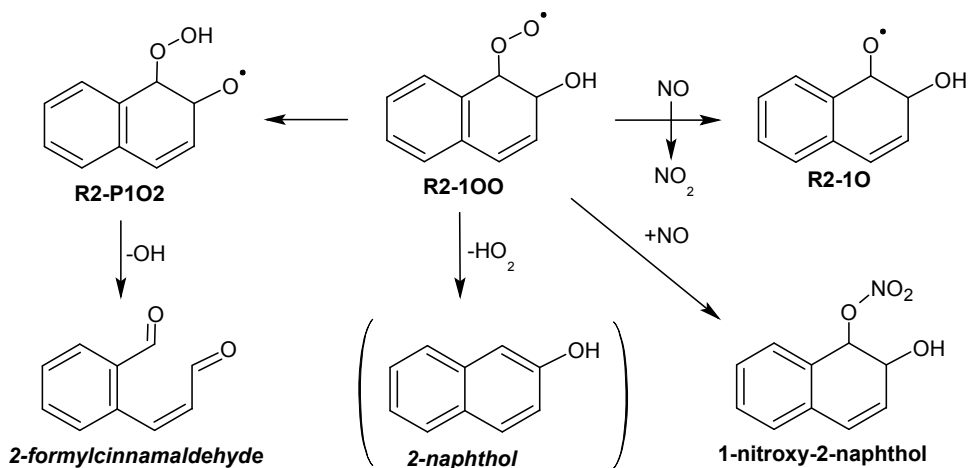
Figure 3.6 *The reaction sequence of peroxy radical R2-1OO under atmospheric condi-
tions proceeds either unimolecularly, or with NO. Possible closed shell reaction products
are 2-formylcinnamaldehyde, 1-nitroxy-2-naphthol and possibly 2-naphthol (see text). The
reaction may also lead to the formation of an intermediate alkyl radical product R1-2O.*

As discussed earlier, the bimolecular reaction between the peroxy radical and NO
is often the competitive reaction channel compared to unimolecular reactions. The
reaction proceeds typically as described by equation 3.2, forming alkoxy radicals
R1-2O and *R2-1O*, in the case of *R1-2OO* and *R2-1OO*. The chain reaction for
alkoxy radicals *R1-2O* and *R2-1O* propagates, and is described in section 3.5. Still
considering the reaction between the peroxy radicals *R1-2OO* and *R2-1OO* and NO,
the addition reaction 3.5 may also be possible, forming *2-nitroxy-1-naphthol* and *1-
nitroxy-2-naphthol* as a result. The described reaction pathways for peroxy radicals
R1-2OO and *R2-1OO* are shown in figures 3.5 and 3.6, respectively.

In addition to the aforementioned bimolecular reactions, the reactions 3.8, 3.9 and
3.10 between two peroxy radicals may also be possible, especially in conditions where
the radical concentration (or rate of formation) is high. For the sake of an example,
let us consider the reaction between *R1-2OO* and a general peroxy radical RO_2.
Now reaction 3.8 will lead to the formation of either a hydroxyketone *R1-2CHO* or
a diol *R1-2OH*, reaction 3.9 to a dimer structure *R1-2OOR* with an oxygen bridge
between the two parent molecules, and reaction 3.10 will leave an alkoxy radical *R1-
2O* similar to reaction 3.2 between RO_2 and NO. The reactions between *R1-2OO*
and RO_2 are shown in figure 3.7. Similar reactions are possible for *R2-1OO*, while
RO_2 may be any available peroxy radical, originating from naphthalene or not.
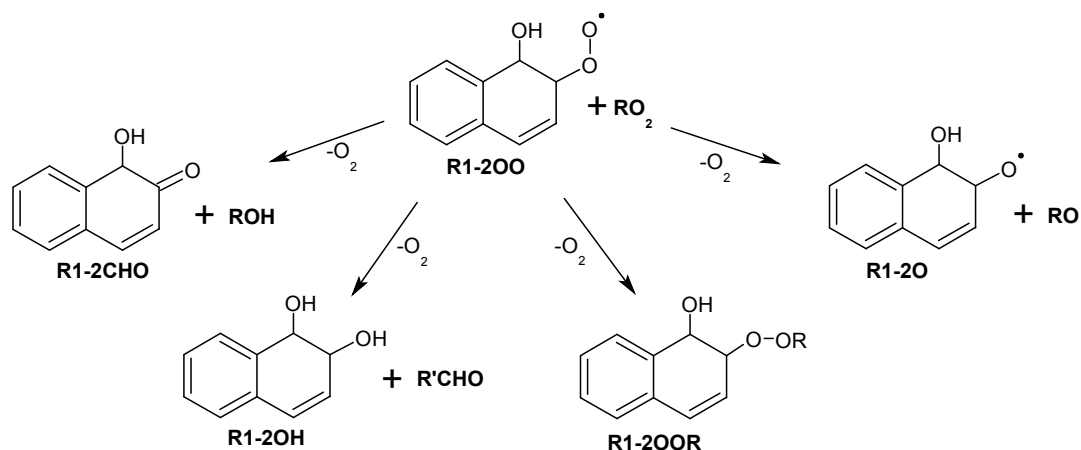
Figure 3.7 *Reactions of peroxy radical R1-2OO with another peroxy radical (RO$_2$) may terminate the reaction sequence of both radicals or allow them to continue by reduction to alkyl radicals. The formation of an oxygen bridge between the two radicals (R1-2OOR) may double the size of the molecule, if the radicals are of same size.*

3.5 Alkoxyradical reactions

As discussed in earlier sections, some of the peroxy radicals (*R1-2OO*, *R2-1OO*) formed in the first steps of the oxidation sequence are reduced to alkoxy radicals (*R1-2O*, *R2-1O*) in bimolecular reactions with either NO or another peroxy radical. In this section we shall discuss the fate of these alkoxy radicals.

Radical *R1-2O* may isomerize to form a bicyclic alkylradical *R1-23O*, which then undergoes another O$_2$ addition and reduction to an alkoxyradical *R1-23O-4O*. The formed radical is likely to abstract a hydrogen atom forming a C$_{10}$H$_8$O$_3$ product. (Zhang et al. 2012) Alternative pathway was suggested by Qu et al. (2006), where radicals *R1-2O* and *R2-1O* would break the bond between C$_1$ and C$_2$, and subsequently decompose to form *2-formylcinnamaldehyde*. Zhang et al. (2012), however, concluded this channel to be highly unlikely due to the high bonding energy between the carbon atoms. Alternative reaction channels for *R2-1O* could not be found from literature. The proposed propagation channels for alkoxyradicals *R1-2O* and *R2-1O* are shown in figure 3.8.

3.6 Radical R1-29OO

The fate of the bicyclic alkylradical *R1-29OO* proposed to form by isomerization of the peroxy radical *R1-2OO*, is currently not known. However, the reactions of a radical with similar structure formed in benzene oxidation (*R26* in figure 3.9) have
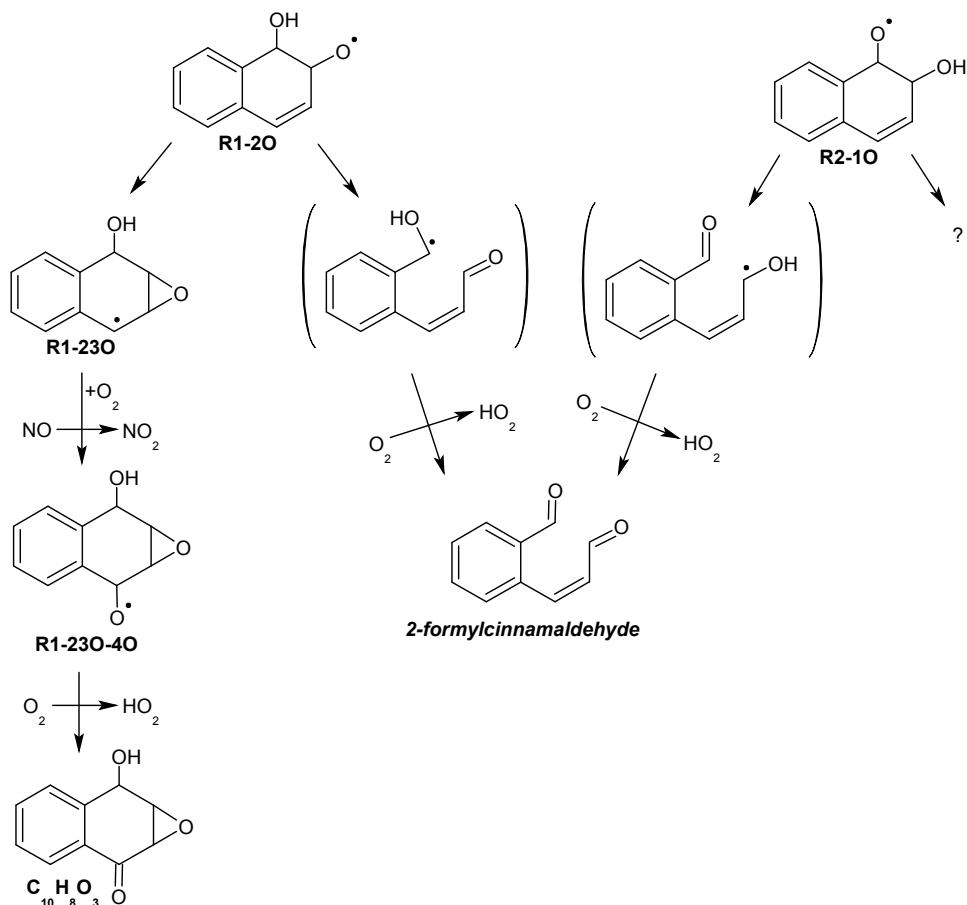
Figure 3.8 *Proposed reaction channels for alkoxy radicals R1-2O and R2-O. There is disagreement in the literature about the plausibility of the 2-formylcinnamaldehyde producing channel. Alternative reaction channels for R2-1O were not found from existing literature, while R1-2O has been proposed to form $C_{10}H_8O_3$ closed shell product.*

been studied, and by assuming similar reaction pathways are possible for *R1-29OO*, we can speculate the outcome of this reaction channel (Zhang et al. 2012).

For benzene originating radical *R26* under atmospheric conditions, 95 % of the time the reaction propagates by the addition of O_2 (Wang et al. 2013), and thus we expect this to be the major channel also for *R1-29OO*. For *R1-29OO*, its resonant structure theoretically allows the formation of *R1-29OO-iOO*, where $i = 3, 6, 8, 10$. It is not in the scope of this study to determine the feasibility of the different positions, so we will have to assume addition to position 3, following the reaction pathway proposed for benzene radical *R26* (figure 3.9).

The O_2 addition to *R26* forms another peroxy radical, that most likely reduces to an alkoxyradical, which in 67 % of the cases isomerizes to accept one more O_2 addition after which it decomposes to form *glyoxal* and *2,3-epoxybutanedialdehyde*. The remaining 33 % decompose already after the first O_2 addition to *glyoxal* and

butanedialdehyde (Wang et al. 2013). The described reaction pathways for benzene radical *R26* are shown in figure 3.9
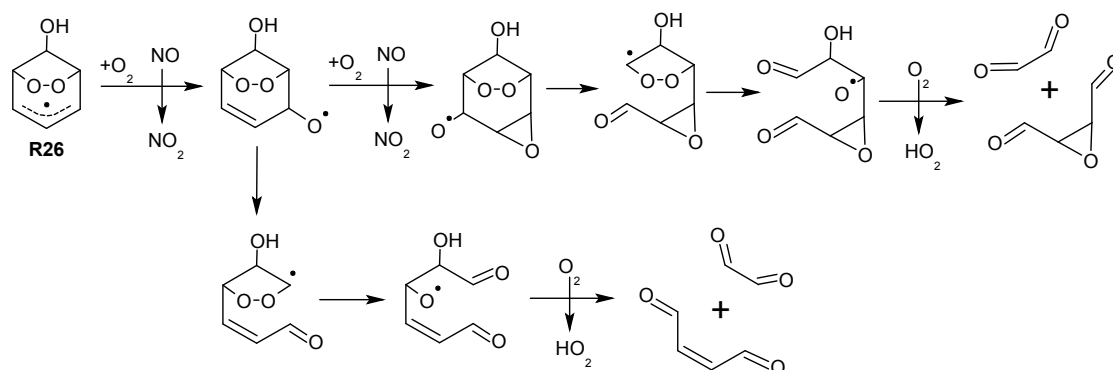

Figure 3.9 *Reactions of peroxy radical R26 formed in benzene oxidation, similar to the radical R1-29OO originating from naphthalene. The reactions of R1-29OO have not been studied in detail, so the best available guess is to deduce them from the known reactions of R26.*

Similar pathway in naphthalene oxidation would first lead to the formation of *R1-29OO-3OO*, as discussed earlier. It will presumably react with another radical in the atmosphere, but unimolecular isomerization reactions cannot be ruled out. The reaction that best explains the measured reaction product yields in benzene oxidation is with NO (Wang et al. 2013), and thus it is expected to be an important pathway also for *R1-29OO-3OO*. In figure 3.10 the speculative reaction pathways for *R1-29OO* are presented. Two branches are shown, the reduction of *R1-29OO-3OO* to an alkoxyradical *R1-29OO-3O* by NO and following decomposition steps adapted from figure 3.9, and reaction with another peroxy radical where either *R1-29OO-3OH* or *R1-29OO-3CO* would be formed. As discussed earlier, these are only speculative reaction pathways for the radical *R1-29OO*.

3.7 Oligomerization

A large fraction of SOA formed in the oxidation of aromatic hydrocarbons, as well as some monoterpenes, has been shown to consist of polymers. Kalberer et al. (2004) showed that 50 % of the SOA mass originating from trimethyl-benzene is polymers with molecular weight ≤ 1000 u. Heaton et al. (2007) studied the ozonolysis of certain monoterpenes, and saw oligomerization in timescale of seconds. In the mentioned studies, the products were identified from the particle phase. In a more recent study, Sakamoto et al. (2013) determined by a direct measurement that the ozonolysis products of ethylene form oligomers in the gas phase, which then partition into the particle phase. Gomez et al. (2015) found evidence of SOA formation
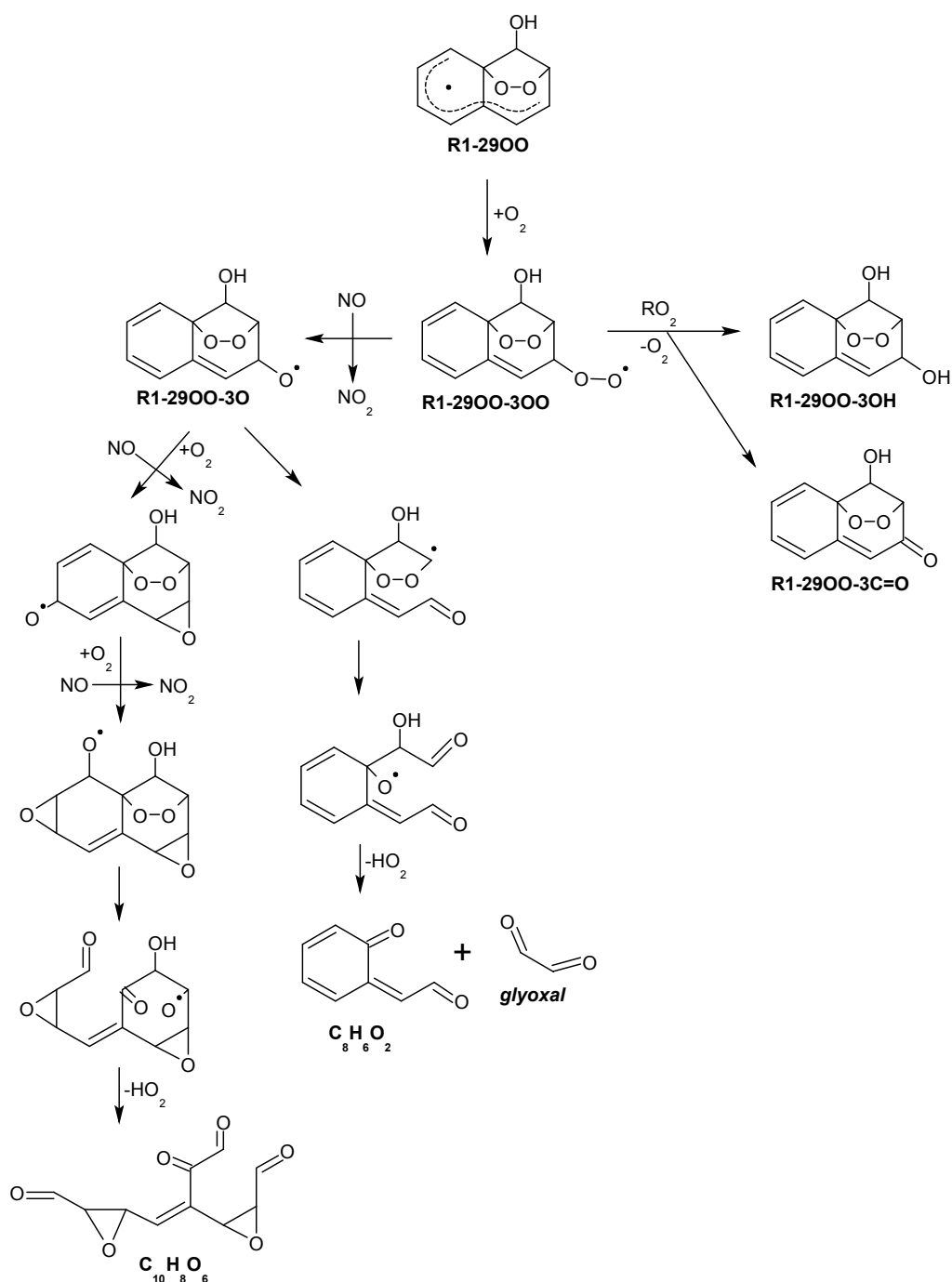
Figure 3.10 *Proposed reactions of peroxy radical R1-29OO, deduced from the reactions of a similar but simpler peroxy radical R26 formed in the oxidation of benzene.*

by heterogeneous oligomerization of glyoxal on the surface of hygroscopic particles. Based on the aforementioned discoveries, it seems that oligomerization reactions may play a major role in the formation of secondary organic aerosol. The dimers – and possibly higher order oligomers – of relatively large molecules have very low saturation vapor pressures. Heaton et al. (2007) estimated the saturation vapor

pressures of monoterpene dimers with computational methods, getting $< 10^{-8}$ Torr for all of the dimers studied. The result suggests that the molecular structures or concentrations of individual dimer species are not necessarily important considering SOA formation, but rather the total concentration of the dimer (or other sufficiently low volatility) species.

References concerning the oligomerization of naphthalene oxidation products could not be found from the literature. However, as discussed in section 3.4, two naphthalene originated peroxy radicals may react with each other, according to reaction 3.9 general to peroxy radicals, forming a dimer compound with an oxygen bridge in between the two monomers. This reaction terminates the oxidative chain reaction and thus does not allow the further formation of higher order oligomers. There may still be one or more unsaturated double bonds in the dimer product though, which allows for another initiation by OH and the formation of a new peroxy radical by O_2 addition. This may then react with another peroxy radical (reaction 3.9) to form a higher order oligomer. The peroxy radicals formed in naphthalene oxidation (*R1-2OO*, *R2-1OO*, *R1-29OO-3OO*) do contain double bonds susceptible to an attack by OH. In figure 3.11 a possible dimerization reaction for *R1-2OO* is presented.
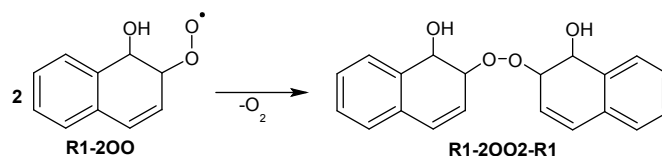

Figure 3.11 *Dimerization reaction between two peroxy radicals R1-2OO, forming the closed shell product R1-2OO2-R1.*

Kalberer et al. (2004) proposed a polymerization mechanism for trimethyl-benzene oxidation products, where the monomer is either methyl-glyoxal or glyoxal, with possible additions of carboxylic acid or other carboxyl compounds. The weak acids formed in the reaction are sufficient to catalyze the reaction. Similar polymerization reaction is expected to contribute to naphthalene SOA formation potential, because glyoxal is formed as a first generation oxidation product in 3–5 percent molar yield. (Nishino et al. 2009).

4.   EXPERIMENTAL

The experimental part of the study was conducted in two parts. A flow tube experiment to qualitatively study the oxidation products of naphthalene was performed in the laboratory of University of Helsinki Division of Atmospheric Sciences. The second part was conducted in the Aerosol physics laboratory of Tampere University of Technology, where the secondary aerosol formation potential of naphthalene was studied by means of an oxidation flow reactor.

4.1   Flow tube measurement

An flow tube experiment to determine the chemical composition of highly oxidized products formed in the OH initiated oxidation of naphthalene was carried out at the University of Helsinki laboratory. A *CI-API-TOF mass spectrometer* with NO_3^- ionization scheme was used to characterize the reacted species. The operation principle of the instrument is discussed in section 4.2. A quartz glass flow tube was used as the reactor, with a residence time of approximately 15 seconds, determined by the inlet flow of the instrument. The OH radicals were produced by introducing water vapor, generated by bubbling N_2 through milli-Q water, into the flow tube and using a 185 nm UV lamp at the end of the reactor to photolyze it according to reaction 4.1.

$$H_2O + hv(\lambda = 185 \text{ nm}) \rightarrow H + OH \tag{4.1}$$
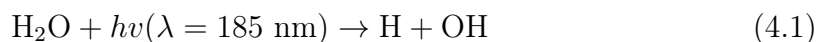
Quantification of the amount of OH radicals produced is not possible with the used instrumentation, and thus the data can only be used for qualitative analysis of the oxidation products. Naphthalene was injected into the reactor by passing a controlled N_2 flow through a closed vial containing a few flakes of solid naphthalene, and synthetic air was used as bath gas in the flow tube.

4.2   CI-API-TOF

Chemical ionization atmospheric pressure interface time-of-flight mass spectrometer (*CI-API-TOF*) was used to determine the chemical composition of the oxidation
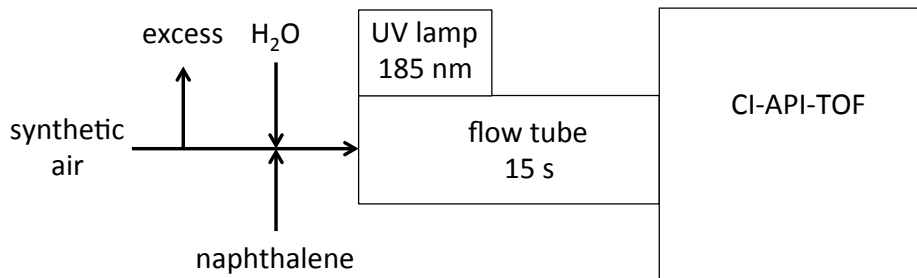
Figure 4.1 *Schematics of the flow tube measurement setup. Water vapor is introduced to produce OH radicals when irradiated with UV light. Naphthalene reacts with OH radicals in synthetic air for approximately 15 seconds before reaching the CI-API-TOF.*

products in the flow tube experiment. The operation principle of the instrument will be discussed next. In short, the molecules in a sample gas flow are first ionized in the *CI inlet*, and then focused into a narrow beam in the *API* as they travel deeper into the instrument and lower in pressure. Finally the beam of ions enter the *TOF* chamber where their mass-to-charge ratio is resolved. The high mass resolving power of the instrument enables the determination of elemental compositions of at least some of the ions reaching the detector, based on their mass defect (Jokinen et al. 2012). For higher masses, the number of different combinations of elements resulting in nearly the same mass defect may become so big that unambiguous solution cannot be found.

The concept of the nitrate CI inlet inlet was first proposed by Eisele & Tanner (1993) to measure gaseous sulfuric acid in the atmosphere with a quadropole mass spectrometer. More recently it has been successfully coupled with a time-of-flight mass spectrometer, making it possible to measure whole mass spectra with high resolution in both mass and time (Jokinen et al. 2012). Nitric acid (HNO_3) is photoionized by an X-ray source in isolation, and the produced nitrate ions (NO_3^-) are then mixed with the sample gas at atmospheric pressure. A specially designed chemical ionization (*CI*) inlet is used to achieve the ionization in controlled manner with minimal wall losses.

Nitrate ions form relatively stable clusters with one or two neutral nitric acid molecules, $(HNO_3)_{1,2} \cdot NO_3^-$. For this reason, nitrate ion is a selective reagent ion. It can only ionize molecules that form energetically more favorable clusters with NO_3^- than neutral HNO_3. Nitrate ion has the tendency to form intermolecular hydrogen bonds and thus H_2SO_4, being a stronger acid than HNO_3, will form even stronger clusters. Thus the ionization scheme is well suited for, but not limited to, the detection of sulfuric acid. Recently a discovery of previously unknown class of highly
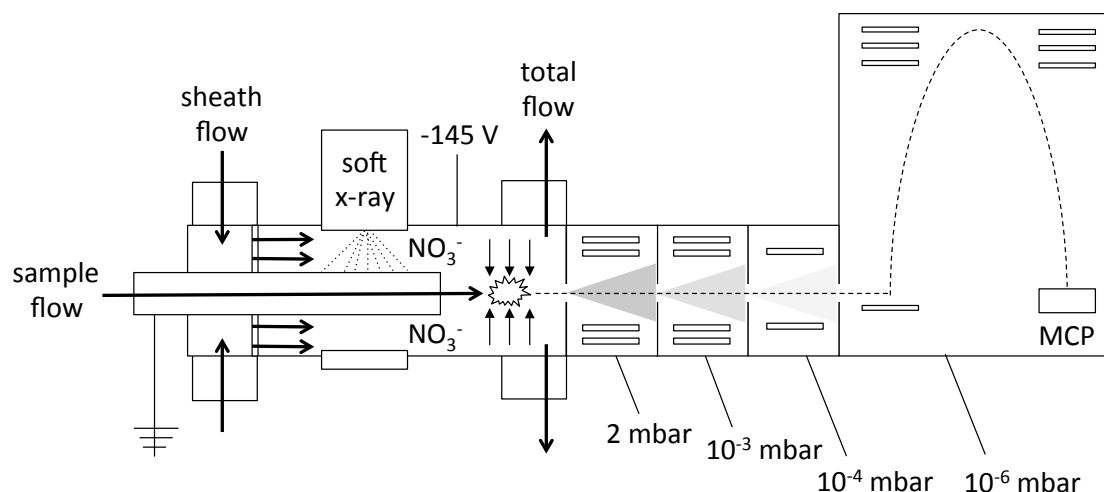
Figure 4.2 *Schematic diagram of the CI-API-TOF. Sample flow (10 lpm) enters the CI inlet through a stainless steel tube into the middle of a concentric laminar sheath flow. The sheath flow (20 lpm) is spiked with HNO_3 (5 mlpm) and irradiated with soft X-rays to produce NO_3^- ions. Once the flows meet, these ions are guided with electric field into the sample flow in the center. Total flow (30 lpm) is sucked out and approximately 0.8 lpm of sample flow enters the APi through a pinhole. The beam of ions is focused and guided through the three chambers of the atmospheric pressure interface, where the pressure is lowered gradually. Finally the ions enter the time-of-flight mass spectrometer, where their mass-to-charge ratio is determined.*

oxidized *extremely low-volatility organic compounds* (*ELVOCs*), in the atmosphere was made with the CI-API-TOF (Ehn et al. 2014).

Hyttinen et al. (2015) showed in a computational study that a hydrocarbon molecule needs to have at least two hydroperoxyl (OOH), or possibly other hydrogen donating (such as OH), functional groups to be able to form stable enough clusters to be detected with the CI-API-TOF. Cyclohexene oxidation products were used in the simulation. It was also shown that too high a concentration of nitric acid in the ionization region or as a contaminant may prevent the sufficient ionization of some of these compounds. The selectivity is an advantage when the goal is to measure certain targeted species, as it allows high sensitivity. The nitrate ion based chemical ionization scheme is well suited for the purpose of this study, as the focus will be on sulfuric acid formation and naphthalene oxidation. It should be kept mind however, that only the highly oxidized organic compounds can be detected, even though they most likely represent only a small minority of the gas phase species.

In between the CI inlet and the TOF-MS there is an *Atmospheric Pressure interface* (*API*), where the pressure is gradually decreased from the atmospheric pressure down to a high vacuum, in the order of 10^{-6} mbar. In the first two chambers there

are quadropoles used to focus the ion beam, but still a major part of the ions get lost along the way. (Junninen 2014)

The actual mass analyzer is a *time-of-flight mass spectrometer* (*TOF*), where the mass-to-charge ration of the sample ions is resolved by measuring their mobility in vacuum. The *atomic mass unit (u)* is defined such that the mass of a single carbon atom (^{12}SC) is exactly 12 u. The mass of a proton is 1.0073 u and neutron 1.0087 u, whereas the mass of an electron is 0.0005 u. However, the exact mass of an atom cannot be calculated simply as a sum of the nuclei masses, because part of the mass goes into the bonding energy between them. The elements with higher mass than carbon have thus a negative mass defect (e.g. sulfur (^{32}S): 31.9721 u) and vice versa (e.g. hydrogen (^{1}H): 1.0078 u). The high mass resolution of the TOF and the unique mass defect of each element ideally enables the determination of elemental compositions of the ions being analyzed. In practice it may be hindered due to overlapping of nearby peaks, or simply due to the number of different combinations possible for high mass ions.

4.3 TSAR measurement

Particle formation process of the oxidation products formed in the reaction between naphthalene and OH radical was studied in an oxidation flow reactor called *TSAR* (TUT Secondary Aerosol Reactor), at the Aerosol physics laboratory of Tampere University of Technology. The reactor consists of a 3.3 dm^3 quartz glass tube surrounded by two dimmable low pressure mercury lamps, emitting UV radiation at 254 nm. The flow rate through the reactor was 15 lpm, resulting in a residence time of approximately 13 seconds. TSAR has been well characterized by Simonen et al. (2016), where they show that the flow profile of TSAR is near laminar, such that the residence time distribution of the sample is narrow. In the paper, OH radicals are produced by mixing H_2O and O_3 into the sample. The ozone is photolyzed in the chamber by UV radiation to produce excited oxygen atoms, $O(^1D)$, which react with water molecules to produce OH. In this study, however, the objective is to study the reaction between naphthalene and the hydroxyl radical. Thus, it would be problematic to introduce other oxidants, such as ozone, into the reactor. A different approach to OH radical generation had to be chosen, and will be discussed next.
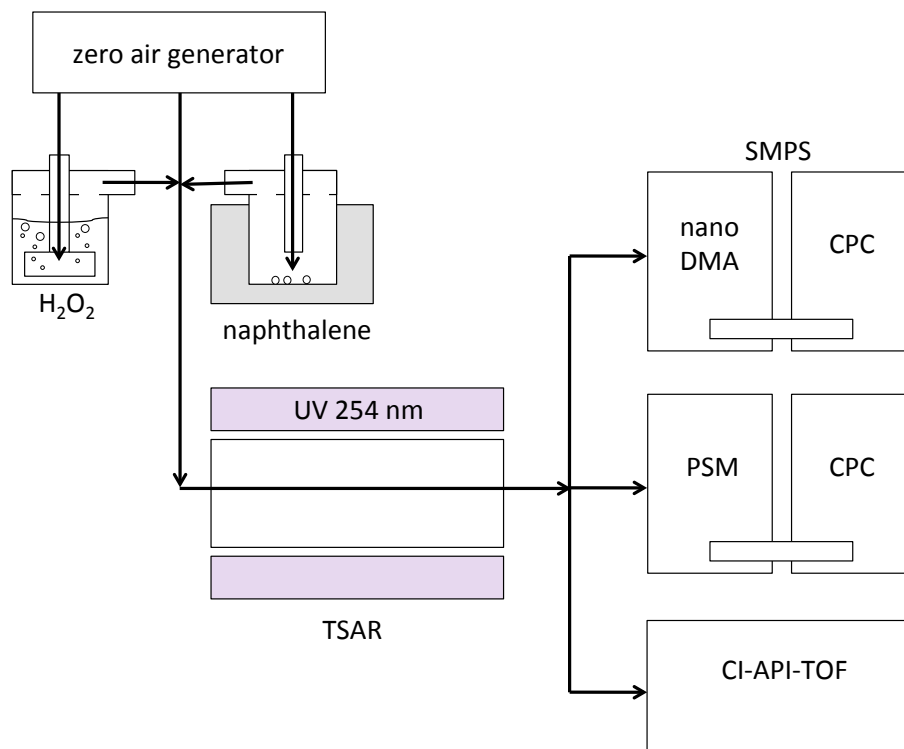
Figure 4.3 *Flow tube measurement setup. Zero air generator was used to purify compressed air used as the bath gas. Hydrogen peroxide and water were introduced to the reactor by bubbling air through their solution. Naphthalene was kept in hot water bath to keep its temperature stable at 70ºC, and carried to the reactor by an air flow. OH radicals were produced in TSAR by UV photolysis of the hydrogen peroxide, where they also reacted with naphthalene for the residence time of approximately 13 seconds. The resulting particles were characterized by means of a nano-SMPS and a PSM, and the gas phase species by a CI-API-TOF.*

4.3.1 OH production and exposure

UV light, at wavelengths $\lambda \geq 248$ nm, photolyzes hydrogen peroxide (H_2O_2) as described by reaction 4.2.

$$H_2O_2 + h\nu(\lambda \geq 248 \text{ nm}) \rightarrow 2 \text{ OH}, \tag{4.2}$$
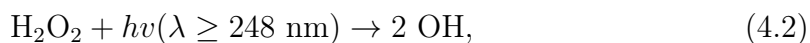
giving rise to two hydroxyl radicals with a quantum yield of unity (Burkholder et al. 2015). This suggests that hydrogen peroxide could be used as an efficient source of OH radicals in TSAR.

Hydrogen peroxide (H_2O_2) was introduced into TSAR by bubbling nitrogen (N_2) through 30% aqueous solution of H_2O_2. The partial pressure of hydrogen peroxide above such solution at 30ºC is 0.65 mmHg (Giguère & Maass 1940), which can be

used to calculate the concentration of H_2O_2 in the flow of gas passing through it. From the ideal gas law, the saturation concentration of H_2O_2 in vapor phase is

$$c_{H_2O_2} = \frac{n}{V} = \frac{p_{H_2O_2}}{kT}, \tag{4.3}$$

where $p_{H_2O_2}$ is its partial pressure, k Boltzmann constant and T temperature. Equation 4.3 gives the concentration of H_2O_2 in the gas bubbled through the solution, assuming it has sufficient time to saturate. To get the concentration inside the reactor, we need to take into account the dilution simply by multiplying with the dilution factor
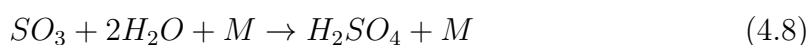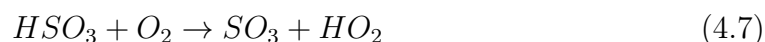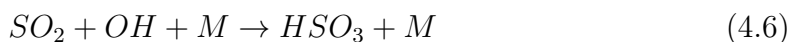
$$D_{H_2O_2} = \frac{Q_{H_2O_2}}{Q_{tot}}, \tag{4.4}$$

which is the ratio of the volumetric flow rate of H_2O_2 into the reactor, $Q_{H_2O_2}$, to the total flow rate Q_{tot}. Using equations 4.3 and 4.4 we get

$$C_{H_2O_2} = D_{H_2O_2} \frac{p_{H_2O_2}}{kT} \tag{4.5}$$

for the concentration of H_2O_2 inside the reactor, $C_{H_2O_2}$, which can be altered by changing the flow rate through the bubbler. The actual temperature of the solution was that of the room (25^oC), instead of 30^oC where $p_{H_2O_2}$ was defined. This will introduce some error to the concentration calculation, and thus the result should be thought of as the upper limit of H_2O_2 in the system.

The direct measurement of hydroxyl radical concentration is a difficult task, but not necessary if we define the *OH exposure (OH_{exp})* of the flow reactor as a product between the mean OH concentration and the residence time. This quantity can be determined indirectly by measuring the change in SO_2 concentration as the sample passes through the chamber, assuming no other loss processes are involved (Lambe et al. 2011). SO_2 reacting with OH radicals leads to the formation of sulfuric acid according to reactions 4.6, 4.7 and 4.8 (Eisele & Tanner 1993), where reaction 4.6 is the rate limiting step for gas phase H_2SO_4 formation. Water vapor needed in reaction 4.8 is provided by the bubbler, and the relative humidity at the end of the reactor was monitored.

$$SO_2 + OH + M \rightarrow HSO_3 + M \tag{4.6}$$

$$HSO_3 + O_2 \rightarrow SO_3 + HO_2 \tag{4.7}$$

$$SO_3 + 2H_2O + M \rightarrow H_2SO_4 + M \tag{4.8}$$

The concentration change of sulfur dioxide due to reaction with the OH radical can be expressed in terms of a differential equation

$$\frac{d[\text{SO}_2]}{dt} = -k_{SO_2+OH}[\text{SO}_2][\text{OH}], \tag{4.9}$$

where k_{SO_2+OH} is the reaction rate coefficient between the two species whose concentrations are $[\text{SO}_2]$ and $[\text{OH}]$. Rearranging equation 4.9 we get

$$-\frac{1}{k_{SO_2+OH}}\frac{d[\text{SO}_2]}{[\text{SO}_2]} = [\text{OH}]dt. \tag{4.10}$$

By setting $[\text{OH}]$ to be the mean OH concentration in the reactor during the period of inspection, and thus independent of time, we can solve the above equation by integrating from $t=0$ to $t=t$

$$-\frac{1}{k_{SO_2+OH}}\int_{[\text{SO}_2]_0}^{[\text{SO}_2]_t}\frac{d[\text{SO}_2]}{[\text{SO}_2]} = [\text{OH}]\int_0^t dt \tag{4.11}$$

$$\frac{1}{k_{SO_2+OH}}\ln\frac{[\text{SO}_2]_0}{[\text{SO}_2]_t} = [\text{OH}]t = OH_{exp}, \tag{4.12}$$

where the resulting equation 4.12 is the OH exposure expressed in terms of SO_2 concentration before and after the chamber and the reaction rate coefficient.

The OH exposure of TSAR was determined experimentally by injecting a constant amount of SO_2 into the reactor with varying amounts of H_2O_2. The UV lights were on at full power during the experiments. Environnement S.A model AF22M SO_2 analyzer was used to monitor the changes in sulfur dioxide concentration and purified air was used as a bath gas. Flow rate through the hydrogen peroxide bubbler was controlled using a mass flow controller, and six points between 10 mlpm and 3000 mlpm were measured for a time period of 15 minutes each. Average concentration of SO_2 during the 15 minute period was calculated, and OH exposure solved from equation 4.12 to give the data points shown in figure 5.2.

4.3.2 Naphthalene oxidation

The reaction between naphthalene and the OH radical was studied with a similar method as described in section 4.3.1. This time, however, naphthalene was injected into TSAR instead of SO_2. Naphthalene (99% purity, obtained from Sigma Aldrich) is solid at room temperature, and its saturation vapor pressure P (bar) can be

expressed using the Antoine equation with parameters $A = 4.27117$, $B = 1831.571$ and $C = -61.329$

$$\log_{10}(P) = A - \frac{B}{T + C},$$ (4.13)

where T is the temperature in Kelvin (NIST 2017). A few flakes of solid naphthalene were inserted in a glass flask which was kept in hot water bath at 70ºC to saturate the vapor phase. Solving equation 4.14 for P at 343.15 K yields

$$P = 10^{A - \frac{B}{T+C}} = 10^{4.27117 - \frac{1831.571}{343.15 - 61.329}} \approx 0.00587 \text{ bar} = 587 \text{ Pa} .$$ (4.14)

A carrier gas flow of purified air through the flask was used to inject the gaseous precursor into TSAR. Again, to calculate the concentration of naphthalene c_{NAP} in the flow assuming it is in saturation, ideal gas law is used:

$$c_{NAP} = \frac{n}{V} = \frac{p_{NAP}}{kT}$$ (4.15)

To make comparable measurement series with the OH exposure measurement (section 4.3.1), naphthalene injection rate was held constant and the OH exposure was altered by changing the flow through the H_2O_2 bubbler. To calculate the concentration of naphthalene inside the reactor, dilution needs to be taken into account. The dilution factor is given by the ratio of naphthalene flow to the total flow

$$D_{NAP} = \frac{Q_{NAP}}{Q_{tot}},$$ (4.16)

and the concentration of naphthalene in TSAR, C_{NAP}, can be obtained by multiplying the carrier flow concentration from equation 4.15 with the dilution factor given by 4.16

$$C_{NAP} = D_{NAP} \frac{p_{NAP}}{kT}.$$ (4.17)

To calculate the amount of naphthalene reacted with OH, we write

$$\frac{d[\text{NAP}]}{dt} = -k_{NAP+OH}[\text{NAP}][\text{OH}],$$ (4.18)

similar to equation 4.9. The reaction rate coefficient is given by equation 3.1. Following the steps of solving 4.9 we get

$$-\frac{1}{k_{NAP+OH}} \int_{[\text{NAP}]_0}^{[\text{NAP}]_t} \frac{d[\text{NAP}]}{[\text{NAP}]} = [\text{OH}] \int_0^t dt,$$ (4.19)

and again by integrating from $t=0$ to $t=t$ we get

$$\frac{1}{k_{NAP+OH}} \ln\frac{[\text{NAP}]_0}{[\text{NAP}]_t} = OH_{exp}, \tag{4.20}$$

where the definition of OH exposure, equation 4.12, was used. Solving for $[\text{NAP}]_t$ yields

$$[\text{NAP}]_t = [\text{NAP}]_0 \exp(-k_{NAP+OH}OH_{exp}), \tag{4.21}$$

The oxidation products of naphthalene are expected to partition between the gas and particle phases. During the experiment, gaseous species were monitored with the CI-API-TOF while scanning mode PSM and a nano-SMPS were used to measure the number size distribution of the particle phase.

5.   RESULTS AND DISCUSSION

The mass spectrum of the naphthalene oxidation products, measured in the flow tube experiment, is shown in figure 5.1 where the identified peaks are shown in blue. The horizontal axis represents the mass-to-charge ratio of the detected species, whereas the vertical axis shows the signal strength in arbitrary units. The reagent ion peaks NO_3^-, $(HNO_3) \cdot NO_3^-$ and $(HNO_3)_2 \cdot NO_3^-$ are seen at 61.9884, 124.9840 and 187.9797 Th, respectively. They are the strongest peaks of the spectrum, extending outside the signal range shown in the figure. Since they carry just one elementary charge, their mass-to-charge ratio in Thomson units (Th) is equivalent to their mass in atomic mass units (u). Same holds true for all the species detected as clusters with the nitrate ion, and thus the horizontal axis is simply referred to as the mass axis from now on.
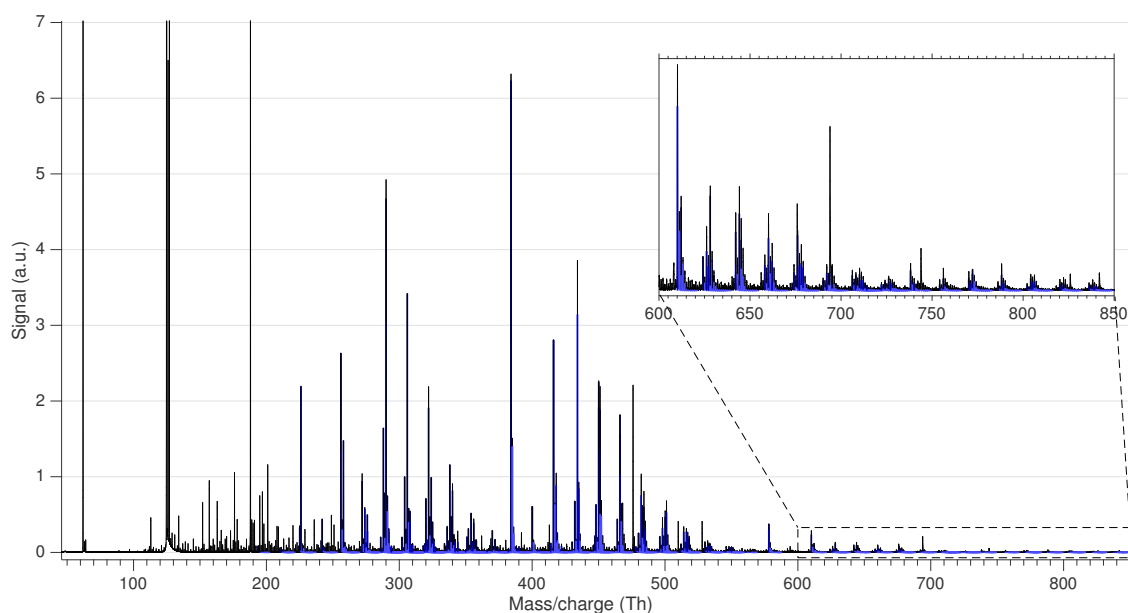

Figure 5.1 *Mass spectrum of the identified ELVOCs, shown in blue color. The horizontal axis is equivalent to the mass of the detected species, since they carry one elementary charge. The vertical axis shows the signal strength in arbitrary units.*

The most abundant peaks identified from the mass spectrum are listed in table 5.1. Monomeric ELVOC species ($C_{10}H_{8-12}O_{4-11}$) form a group of peaks in mass

range from approximately 250 up to around 370 u, as can be seen in the mass spectrum (figure 5.1). Most of the product species contain more than eight hydrogen atoms, suggesting that OH addition is indeed the major pathway of initiation of the oxidation. Less than eight would suggest hydrogen abstraction, since the parent molecule has eight hydrogens. A product molecule having exactly eight hydrogen atoms could have been initiated either way, since depending on the termination reaction a hydrogen atom may be added to or abstracted from the molecule. Some of the monomer products were found to contain 12 or even 14 hydrogen atoms, which would in turn suggest more than one OH addition to the molecule.
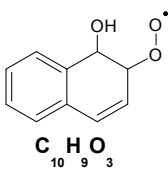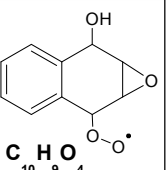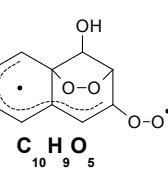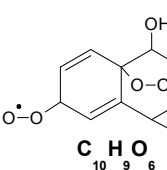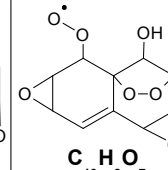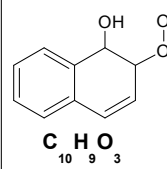
Table 5.1 *List of peaks identified from the mass spectrum as clusters with NO_3^-. The reported masses, in atomic mass units, include the mass of the nitrate ion (61.9884 u).*

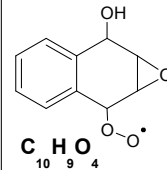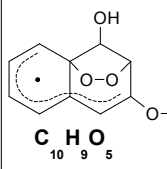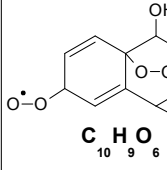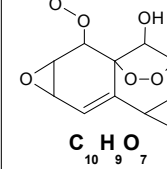| 256.0463	272.0412	274.0568	286.0205	288.0361	289.0439
$C_{10}H_{10}O_4$	$C_{10}H_{10}O_5$	$C_{10}H_{12}O_5$	$C_{10}H_8O_6$	$C_{10}H_{10}O_6$	$C_{10}H_{11}O_6$
290.0518	292.0674	302.0154	304.0310	306.0467	308.0623
$C_{10}H_{12}O_6$	$C_{10}H_{14}O_6$	$C_{10}H_8O_7$	$C_{10}H_{10}O_7$	$C_{10}H_{12}O_7$	$C_{10}H_{14}O_7$
320.0259	322.0416	324.0572	336.0208	338.0365	340.0521
$C_{10}H_{10}O_8$	$C_{10}H_{12}O_8$	$C_{10}H_{14}O_8$	$C_{10}H_{10}O_9$	$C_{10}H_{12}O_9$	$C_{10}H_{14}O_9$
352.0158	354.0314	356.0471	370.0263	384.1089	400.1038
$C_{10}H_{10}O_{10}$	$C_{10}H_{12}O_{10}$	$C_{10}H_{14}O_{10}$	$C_{10}H_{12}O_{11}$	$C_{20}H_{18}O_4$	$C_{20}H_{18}O_5$
416.0987	432.0936	448.0885	464.0834	466.0991	480.0784
$C_{20}H_{18}O_6$	$C_{20}H_{18}O_7$	$C_{20}H_{18}O_8$	$C_{20}H_{18}O_9$	$C_{20}H_{20}O_9$	$C_{20}H_{18}O_{10}$
482.0940	484.1097	496.0733	512.0682		
$C_{20}H_{20}O_{10}$	$C_{20}H_{22}O_{10}$	$C_{20}H_{18}O_{11}$	$C_{20}H_{18}O_{12}$		

At larger masses, from 380 up to around 520 u, ELVOC dimers ($C_{20}H_{18-22}O_{4-12}$) were identified. The strongest product peak of the spectrum is $C_{20}H_{18}O_4$ at mass 384.1089 u. The analysis of the mass spectrum reveals only the elemental composition of the species, and nothing about the molecular structure. However, based on the earlier discussion of possible reaction pathways (chapter 3), it can be stated with high confidence that this product is formed in the reaction between two peroxy radicals, as shown in figure 3.11. Being the dominant product peak, it suggests that this kind of oxidative oligomerization may be significant reaction pathway in naphthalene oxidation, forming low-volatility products in just a few reaction steps. It would then be expected that other peroxy radicals formed in different branches of the reaction sequence also react similarly to form dimers. In table 5.2 the peroxy radicals with distinct elemental composition, expected to form in the reactor, are shown in the first row and column. In the rest of the fields, the mass of the dimer product that would form in the reaction between the corresponding peroxy radicals is shown. The masses include the mass of a nitrate ion and the gray fields denote duplicate structures. Comparison of tables 5.1 and 5.2 suggests that all the possi-

ble combinations based on the reaction mechanism are also observed in the mass spectrum. It should be once again noted though, that while the elemental compositions are the same, the molecular structure may be different – which is obvious just looking at table 5.2 where the same mass may represent two or three different structures. It is also worth noting that the formation rate of these dimer products strongly depends on the concentration of the peroxy radicals acting as precursors, and thus the results of this laboratory experiment may have limited generalizability to other scenarios.

Table 5.2 *Proposed ELVOC dimer structures and their masses, as detected clustered with the nitrate ion: $m_{NO_3} = 61.9884$.*

	$C_{10}H_9O_3$	$C_{10}H_9O_4$	$C_{10}H_9O_5$	$C_{10}H_9O_6$	$C_{10}H_9O_7$
$C_{10}H_9O_3$	384.1089	400.1038	416.0987	432.0936	448.0885
$C_{10}H_9O_4$	400.1038	416.0987	432.0936	448.0885	464.0834
$C_{10}H_9O_5$	416.0987	432.0936	448.0885	464.0834	480.0784
$C_{10}H_9O_6$	432.0936	448.0885	464.0834	480.0784	496.0733
$C_{10}H_9O_7$	448.0885	464.0834	480.0784	496.0733	512.0682

Even further up the mass axis, also trimer and tetramer species are observed, as seen in the zoomed in part of the spectrum in figure 5.1. However, their signal is rather low and the uncertainty in identification of the elemental composition rather

big, and thus they are not listed in table 5.1. Nevertheless, they do support the finding of oxidative oligomerization being a significant reaction pathway, suggesting that also higher order oligomers may form in the reaction sequence, as was speculated in section 3.7. The comparatively low signal of these peaks may partly be explained by the mass dependent transmission of the mass spectrometer, as well as the rather short residence time in the flow tube. Furthermore, these species likely have several orders of magnitude lower saturation vapor pressure compared to the parent molecule, which makes them more prone to condensational losses. Particle instrumentation was not utilized in the flow tube experiment.

In the TSAR experiment, the OH exposure of the oxidation flow reactor as a function of the H_2O_2 flow was calibrated using SO_2, as discussed in section 4.3.1. The results are presented in figure 5.2. There is clearly a linear relationship between the OH exposure and H_2O_2 flow, maintaining linearity up to the highest flow rate used in the measurement. This suggests that even with the higher flow rates, the bubbling gas can be assumed saturated with hydrogen peroxide. The determined OH exposures are of comparable magnitudes to those measured by Simonen et al. (2016), where a different method (O_3 photolysis) was used for OH production.
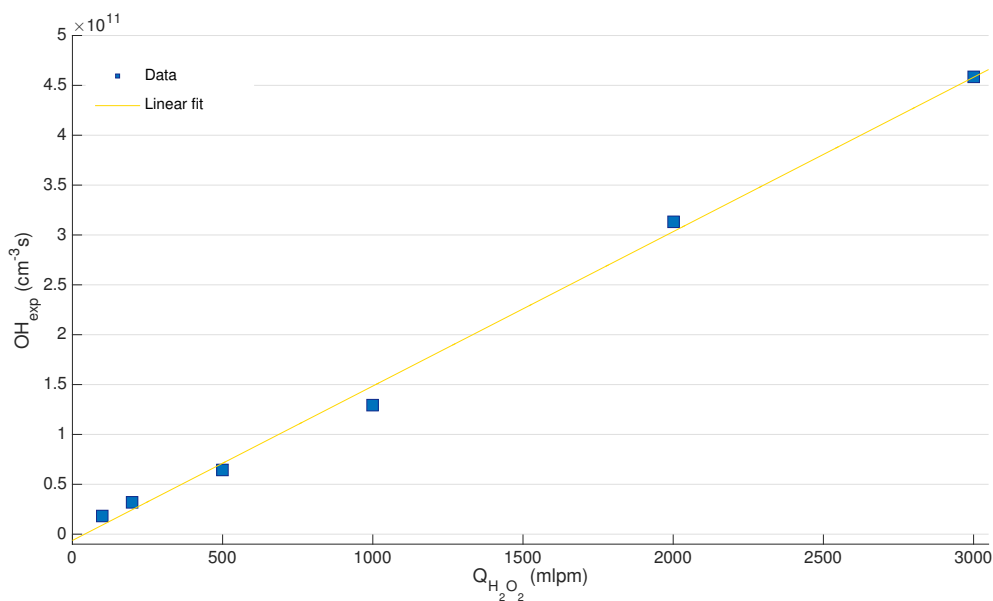
Figure 5.2 *Determining the OH exposure as a function of hydrogen peroxide (H_2O_2) flow rate. There is clearly a linear relationship between the H_2O_2 feed rate and the resulting OH exposure.*

The ELVOC concentration, measured with the CI-API-TOF as a function of the OH exposure, is presented in figure 5.3. The instrument was not calibrated for concentration, and thus absolute concentrations cannot be resolved. The shown total ELVOC signal (green markers) is calculated as the sum of all the identified

peaks in the mass spectrum. To assess the ratio of monomers (red markers) and higher order oligomers (blue markers) contributing to the total signal, a division was done according to table 5.2 such that the signal in mass range 250 to 370 u was attributed to monomers and 370 to 600 u to higher order oligomers. The zero level of the vertical axis in figure 5.3 is set to the background level, measured with naphthalene feed and UV light on but H_2O_2 feed turned off. It can be seen that even with the lowest OH exposure the signal is significantly above the zero level, and thus the measured signal is clearly originating from the OH oxidation products of naphthalene. As the OH exposure is increased, the monomer concentration starts to grow rapidly, whereas the oligomer concentration decreases. The total concentration shows a clear increase between the first four measurement points. At the fourth point it reaches a plateau after which the increase of OH exposure affects neither the total concentration nor the ratio between monomers and oligomers. The oligomer to monomer ratio in this experiment changes from an initial ratio of approximately 1:2 down to about 1:4. To explain this behavior, a deeper understanding of the underlying chemistry is needed. The reason to the plateau of the total ELVOC signal, however, is obvious if we look at figure 5.4.
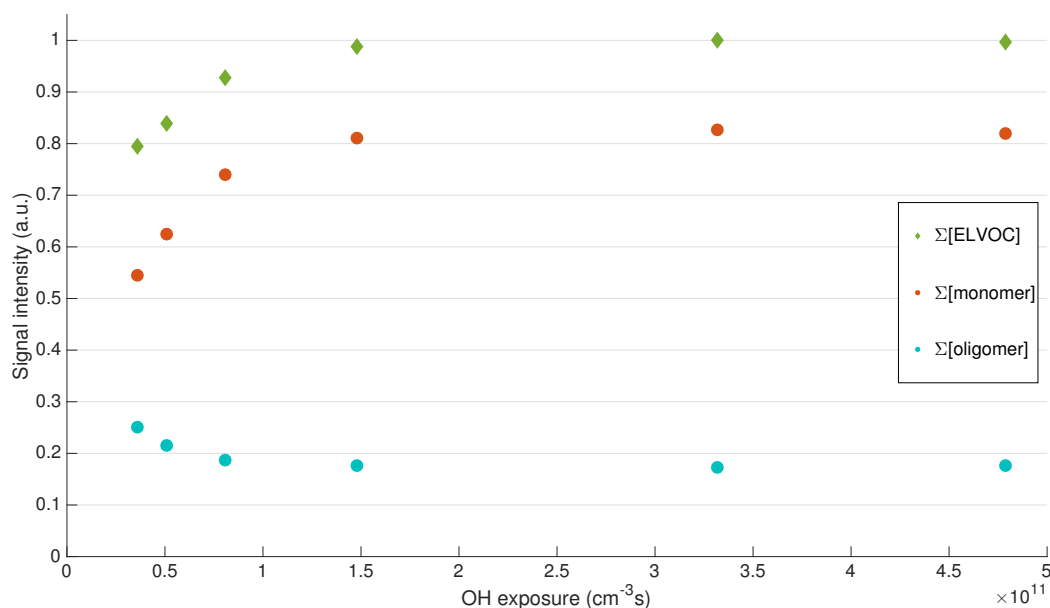
Figure 5.3 *ELVOC concentration (in arbitrary units) as a function of OH exposure in the TSAR experiment. Green markers show the total signal, whereas the red and blue markers represent the part attributed to ELVOC monomers and oligomers, respectively. Zero level is set to the corresponding signal level during the zero measurement. The total concentration grows rapidly as the OH exposure is increased from zero, but soon reaches a plateau. The ratio of oligomers to monomers is initially approximately 1:2, but decreases down to 1:4 as the OH exposure is increased.*

In figure 5.4 the amount of naphthalene reacted with the OH radical, calculated per equations 4.15 and 4.21, is plotted against the OH exposure of TSAR. The initial naphthalene concentration, as given by the equation 4.15, is indicated by the red dashed line. From the figure we see that the lowest OH exposure corresponds to approximately half of the naphthalene reacting with OH. Going higher in OH exposure, the fourth data point corresponds already to over 90% consumption of naphthalene. In the last two data points, essentially all of the naphthalene reacts with OH, and thus there is excess OH in the system. This is likely to induce second generation reactions – that is – a second initiation of the already reacted products due to the free OH radicals. This may be one explanation to the observed decrease in oligomer concentration, discussed earlier in relation to figure 5.3, since the oxidation will ultimately lead to fragmentation of the carbon backbone of the molecule.
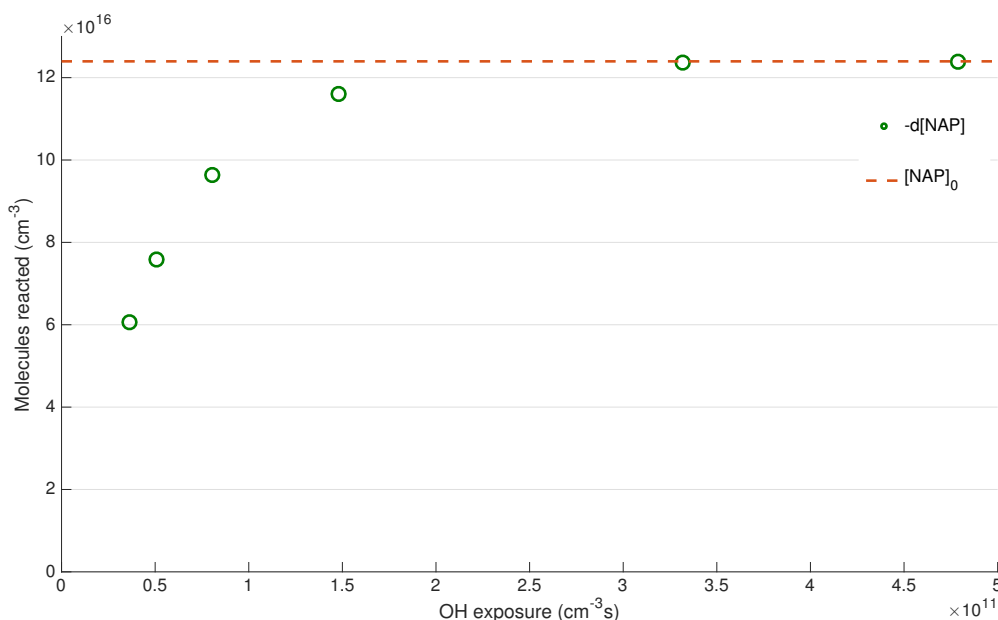
Figure 5.4 *Reacted naphthalene as a function of the OH exposure. Starting from the lowest OH exposure, at the fourth data point already more than 90% of the naphthalene reacts with OH. Essentially all of the naphthalene reacts with OH with the highest exposures used in the measurement. This leaves free OH radicals in the system, most likely reacting with some of the oxidation products, producing second generation products.*

Secondary aerosol particles formed in TSAR were characterized with a PSM in scanning mode and an SMPS. The number size distributions measured by both of these instruments are combined in figure 5.5. PSM data shows a large number of very small particles (or clusters), in the size range 1–3 nm. The data suggests this distribution to be bimodal, having the first mode at around 1.5 nm and the second at approximately 2 nm. SMPS size distributions show a single mode at approximately 6 nm – the exact mode of each distribution is marked with a diamond in the figure, and

is observed to have a growing trend with increasing OH exposure. The total number concentration is increasing as well. There seems to be some discrepancy between the PSM and SMPS distributions where they overlap, even though some of the SMPS distributions seem to show signs of a second mode of particles around 2 nm, similar to the PSM. Unfortunately there is not enough overlap to really draw conclusions. The discrepancy may be due to the lower size cutoff of the SMPS. Interestingly, even though nearly all of the naphthalene is consumed already at the fourth data point as discussed earlier, the increased OH exposure is still clearly reflected in the SMPS distributions. This suggests that functionalization is still the dominant oxidation pathway with the higher OH exposures, as opposed to fragmentation. Particle phase chemistry may also be involved.
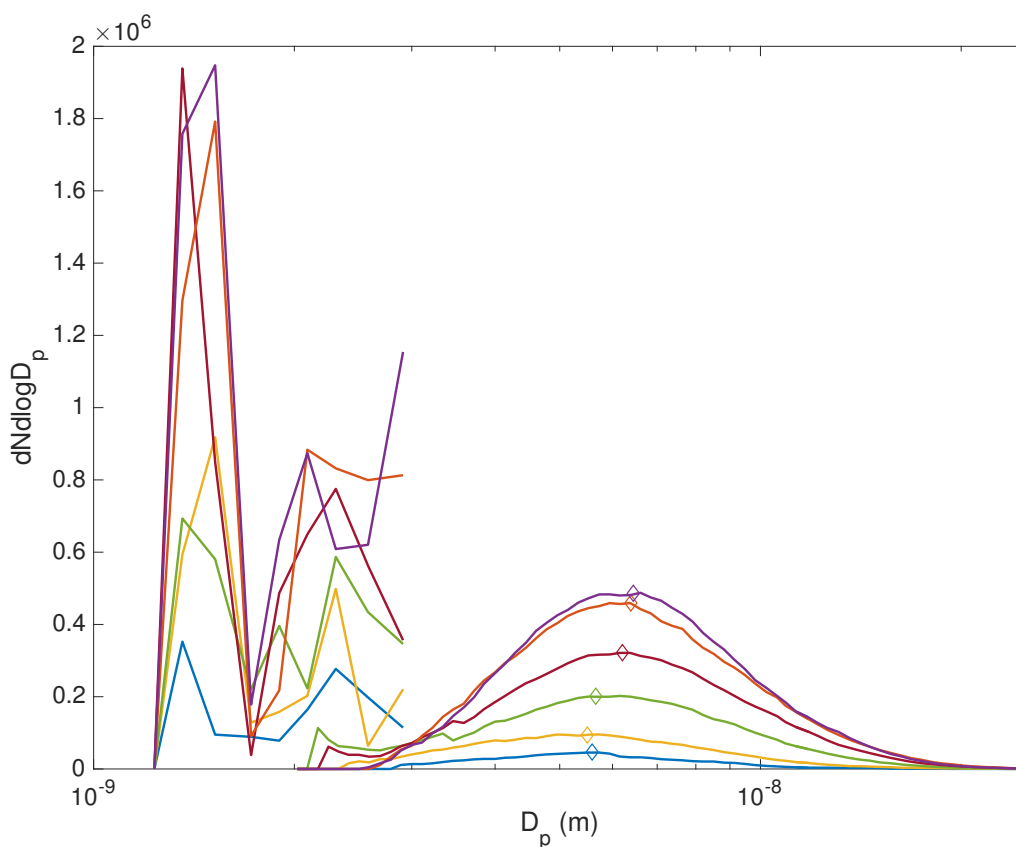
Figure 5.5 *Particle number size distributions of naphthalene SOA measured by PSM and SMPS. PSM measures the distribution at the smallest sizes (1–3 nm) whereas the range of SMPS extends from 2 up to 20 nm. The total particle number concentration increases as the OH exposure is increased. The increase in the number of the very small particles is fastest with the relatively low OH exposures. The SMPS distributions show a growing trend of the modes, marked with diamonds.*

The total particle number concentrations measured by PSM and SMPS are shown in figure 5.6 as a function of the OH exposure. It can be seen that the number of very small particles (in PSM size range) grows faster compared to the slightly

larger particles measured by SMPS. The result suggests that the oxidation products of naphthalene readily nucleate to form new particles. Whether the nucleation process is homogeneous cannot be stated with confidence, because there is always a small background concentration of sulfuric acid (as well as other impurities) in the system, which might participate in the initial steps of particle formation. Before the experiment, the reactor was cleaned with acetone to remove any organic contaminants. Still the role of contaminants potentially participating in the particle formation cannot be ruled out.

After the measurement series was completed, the H_2O_2 flow was turned off to stop the OH production in order to measure the zero level of particle number concentration (and ELVOC concentration, as discussed earlier). The concentration was observed to rapidly decrease immediately after the OH production was stopped, and then slowly decay further down as the reactor was being flushed, with both the UV light and naphthalene flow still on. After about 20 minutes of flushing, the zero level was recorded and is shown in figure 5.6 for both PSM and SMPS. From this figure, it is clear that OH oxidation is the dominant process governing the new particle formation in this experiment. It is worth noting, that the particle number concentration keeps growing until the highest OH exposures, even though there is no more naphthalene to be oxidized. This might suggest that also some of the second generation oxidation products are potential sources of secondary aerosol, which is not unexpected. The other possible explanation is that there are some contaminants in the system, that get oxidized and contribute to the particle formation.

To evaluate the credibility of the acquired results, let us approximate the condensable vapor concentration required to generate the observed particle growth rate from the nucleation mode measured by PSM, to the SMPS size range. This can be done according to equation 2.13. The challenge is that many of the properties of the gas phase species in question are not known, and thus the accuracy of the approximation is uncertain. Still, at least we can get an order of magnitude estimate. We set the condensed phase density of the vapor to that of water, 1 g/cm^3, vapor molecule diameter to 0.5 nm, mass accomodation coefficient to unity and mass of the vapor molecule to the weighted average of the measured mass spectrum, ~300 u. Finally, by setting the temperature to 298 K, initial particle size to 1.5 nm and final to 6 nm, and growth time to the residence time of TSAR, 13 seconds, the evaluation of equation 2.13 yields $C_v = 7.3 \cdot 10^9$ cm^{-3}. This is the required concentration of condensable vapor molecules to achieve the observed particle growth rate. From figure 5.4 we note that at the lowest OH exposure, approximately $6 \cdot 10^{16}$ cm^{-3} radicals are generated in the system. This means that 1 in 10^7 of these radicals must form condensable oxidation products, to satisfy the condition given by equation 2.13.
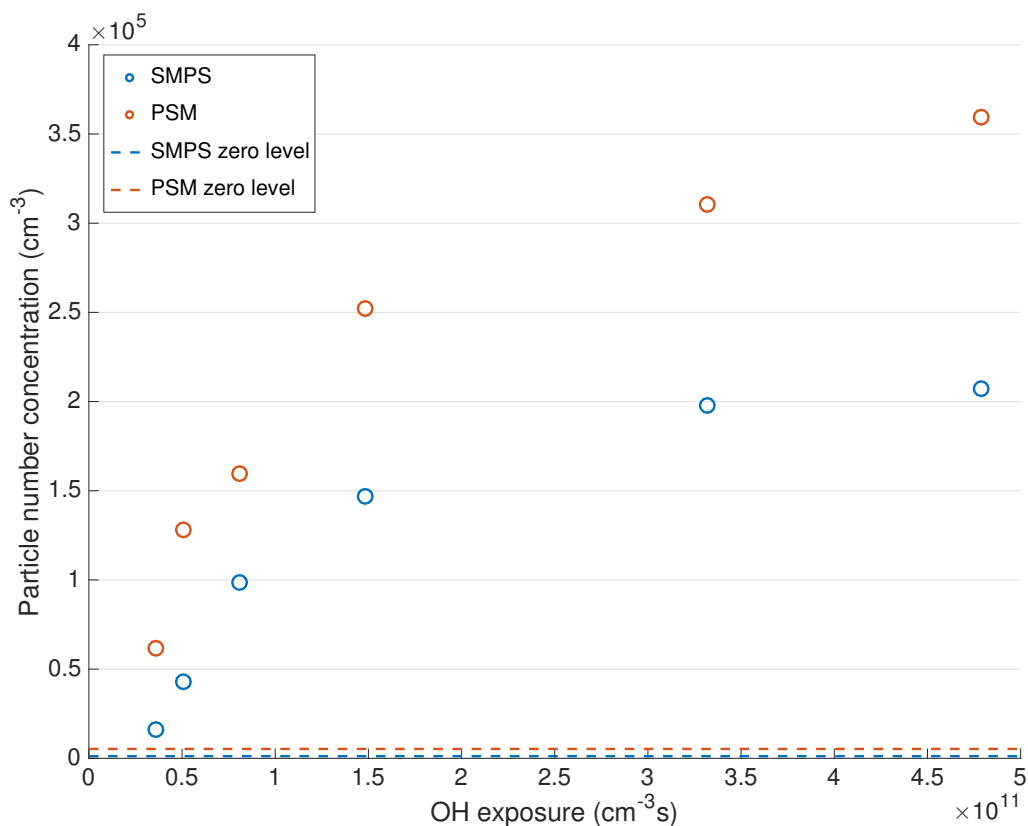
Figure 5.6 *Particle number concentration of naphthalene SOA in TSAR as a function of OH exposure, as measured with PSM and SMPS. The zero levels of both instruments are shown with dashed lines.*

What is lacking from the previous analysis, though, is a description of the formation of the initial 1.5 nm diameter particles – the nucleation rate. Detailed modeling of the aerosol dynamics in the system is beyond the scope of this thesis. However, inferring from the previous analysis of condensational growth rate, the aforementioned 10^7 radicals cm^{-3} would have to suffice to produce the observed number concentration of the 1.5 nm particles for the ends to meet. From figure 5.6 we note that the number concentration of these nucleation mode particles is in the order of 10^5 cm^{-3}, meaning that approximately 1 % of the initiated oxidation reactions would lead to a product that will readily nucleate. Further studies are needed for more detailed analysis, and to rule out the role of contaminants in the nucleation.

6. CONCLUSION

Secondary organic aerosol formation mechanism of a polycyclic aromatic hydrocarbon – naphthalene – in reaction with the OH radical was studied theoretically, by making a literature survey on the reaction mechanisms, and experimentally in two different laboratory setups. The aim was to identify some of the low volatility gas-phase reaction products subject to nucleation and condensation, and the reaction mechanisms leading to their formation. The first experiment was targeted to characterization of the products, whereas the aim of the second experiment was to show that these products can form particles.

Qualitative analysis of the oxidation products was done in a flow tube experiment, performed in the University of Helsinki laboratory, by utilizing the CI-API-TOF mass spectrometer with NO_3^- ionization scheme. Extremely low-volatility organic compounds were identified from the mass spectrum. Naphthalene was found to produce oligomeric structures in the process of oxidation, likely due to the formation of an oxygen bridge (–OO–) between two peroxy radicals ($RO_2\cdot$). The dominant product peak in the mass spectrum was found to correspond to this kind of a dimer composition, suggesting that this is potentially an important reaction pathway in the formation of low-volatility products in just a few reaction steps – in timescale of seconds. Higher order oligomers were also identified, but their formation by the suggested mechanism requires a second initiation by OH. The existing literature concerning the reaction mechanisms between naphthalene and OH was reviewed, and while some of the found products could be explained by the already recognized mechanisms, further research is clearly needed in order to gain a better understanding of the formation of the highly oxidized species observed.

The second experiment was conducted in the aerosol physics laboratory at Tampere University of Technology, where an oxidation flow reactor – TSAR – was used to study the particle formation potential of naphthalene oxidation products. Particle instrumentation (PSM and SMPS) was used to measure the number size distribution of the formed particles in sub-10 nm size range. Relative concentration of the gas-phase oxidation products was simultaneously monitored by the CI-API-TOF. The reaction system was found to produce readily nucleating species in timescale of

seconds, forming a large number of sub-3 nm particles measured by the PSM. The SMPS showed a mode of particles approximately 6 nm in diameter. The particle distribution was clearly subject to changes in the OH exposure of TSAR, showing an increase in the particle number as the OH exposure was increased. The qualitative results of this experiment suggest that some of the naphthalene oxidation products in high concentration readily nucleate to form new particles. The role of contaminants in the system, however, could not be ruled out based on the performed measurements. Thus based on the obtained results it remains unclear whether the naphthalene oxidation products are able to nucleate homogeneously, or if contaminants play a significant role in particle formation in the study performed. Future studies should be aimed towards making similar experiments in ultrapure conditions with exhaustive zero measurements, to rule out the role of contaminants. To evaluate the significance of the findings, the measurements should be repeated in atmospherically relevant conditions, with the goal of modeling the aerosol dynamics of the system.

Polycyclic aromatic precursors have recently been recognized as major contributors in urban secondary organic aerosol formation (Chan et al. 2009). The processes governing SOA are still largely unknown, which is one of the great challenges in atmospheric research. This thesis presents new findings on the SOA formation from naphthalene oxidation products, that may be of significance on the way towards quantitative understanding of SOA formation from (poly)aromatic precursors.

BIBLIOGRAPHY

Andersson, J. T. & Achten, C. (2015), 'Time to say goodbye to the 16 EPA PAHs? toward an up-to-date use of PACs for environmental purposes', *Polycyclic Aromatic Compounds* **35**(35), 330–354.

Asa-Awuku, A., Miracolo, M. A., Kroll, J. H., Robinson, A. L. & Donahue, N. M. (2009), 'Mixing and phase partitioning of primary and secondary organic aerosols', *Geophysical Research Letters* **36**(15).

Atkinson, R., & Arey, J. (2003), 'Atmospheric degradation of volatile organic compounds', *Chemical Reviews* **103**(12), 4605–4638.

Atkinson, R. & Arey, J. (1994), 'Atmospheric chemistry of gas-phase polycyclic aromatic hydrocarbons: formation of atmospheric mutagens.', *Environmental Health Perspectives* **102**, 117–26.

Atkinson, R., Arey, J., Zielinska, B. & Aschmann, S. M. (1987), 'Kinetics and products of the gas-phase reactions of OH radicals and N_2O_5 with naphthalene and biphenyl', *Environmental Science & Technology* **21**(10), 1014–1022.

Bloss, C., Wagner, V., Jenkin, M. E., Volkamer, R., Bloss, W. J., Lee, J. D., Heard, D. E., Wirtz, K., Martin-Reviejo, M., Rea, G., Wenger, J. C. & Pilling, M. J. (2005), 'Development of a detailed chemical mechanism (MCMv3.1) for the atmospheric oxidation of aromatic hydrocarbons', *Atmospheric Chemistry and Physics* **5**(3), 641–664.

Bowman, F. M. & Melton, J. A. (2004), 'Effect of activity coefficient models on predictions of secondary organic aerosol partitioning', *Journal of Aerosol Science* **35**(12), 1415 – 1438.

Bunce, N. J., Liu, L., Zhu, J. & Lane, D. A. (1997), 'Reaction of naphthalene and its derivatives with hydroxyl radicals in the gas phase', *Environmental Science & Technology* **31**(8), 2252–2259.

Burkholder, J. B., Sander, S. P., Abbatt, J., Barker, J. R., Huie, R. E., Kolb, C. E., Kurylo, M. J., Orkin, V. L., Wilmouth, D. M. & Wine, P. H. (2015), 'Chemical kinetics and photochemical data for use in atmospheric studies, evaluation no. 18', *JPL Publication 15-10* .

Calvert, J., Atkinson, R., Becker, K., Kamens, R., Seinfeld, J., Wallington, T. & Yarwood, G. (2002), *The Mechanisms of Atmospheric Oxidation of Aromatic Hydrocarbons*, Oxford University Press.

Chan, A. W. H., Kautzman, K. E., Chhabra, P. S., Surratt, J. D., Chan, M. N., Crounse, J. D., Kürten, A., Wennberg, P. O., Flagan, R. C. & Seinfeld, J. H. (2009), 'Secondary organic aerosol formation from photooxidation of naphthalene and alkylnaphthalenes: implications for oxidation of intermediate volatility organic compounds (IVOCs)', *Atmospheric Chemistry and Physics* **9**(9), 3049–3060.

De Gouw, J. & Jimenez, J. L. (2009), 'Organic aerosols in the earth's atmosphere', *Environmental Science & Technology* **43**(20), 7614–7618.

Donahue, N. M., Epstein, S. A., Pandis, S. N. & Robinson, A. L. (2011), 'A two-dimensional volatility basis set: 1. organic-aerosol mixing thermodynamics', *Atmospheric Chemistry and Physics* **11**(7), 3303–3318.

Donahue, N. M., Kroll, J. H., Pandis, S. N. & Robinson, A. L. (2012), 'A two-dimensional volatility basis set – part 2: Diagnostics of organic-aerosol evolution', *Atmospheric Chemistry and Physics* **12**(2), 615–634.

Ehn, M., Thornton, J. A., Kleist, E., Sipilä, M., Junninen, H., Pullinen, I., Springer, M., Rubach, F., Tillmann, R., Lee, B., Lopez-Hilfiker, F., Andres, S., Acir, I.-H., Rissanen, M., Jokinen, T., Schobesberger, S., Kangasluoma, J., Kontkanen, J., Nieminen, T., Kurten, T., Nielsen, L. B., Jorgensen, S., Kjaergaard, H. G., Canagaratna, M., Dal Maso, M., Berndt, T., Petaja, T., Wahner, A., Kerminen, V.-M., Kulmala, M., Worsnop, D. R., Wildt, J. & Mentel, T. F. (2014), 'A large source of low-volatility secondary organic aerosol', *Nature* **506**(7489), 476–479.

Eisele, F. L. & Tanner, D. J. (1993), 'Measurement of the gas phase concentration of H2SO4 and methane sulfonic acid and estimates of H2SO4 production and loss in the atmosphere', *Journal of Geophysical Research: Atmospheres* **98**(D5), 9001–9010.

Friedman, C. L., Pierce, J. R. & Selin, N. E. (2014), 'Assessing the influence of secondary organic versus primary carbonaceous aerosols on long-range atmospheric polycyclic aromatic hydrocarbon transport', *Environmental Science & Technology* **48**(6), 3293–3302.

Fuzzi, S., Baltensperger, U., Carslaw, K., Decesari, S., Denier van der Gon, H., Facchini, M. C., Fowler, D., Koren, I., Langford, B., Lohmann, U., Nemitz, E., Pandis, S., Riipinen, I., Rudich, Y., Schaap, M., Slowik, J. G., Spracklen, D. V., Vignati, E., Wild, M., Williams, M. & Gilardoni, S. (2015), 'Particulate matter, air quality and climate: lessons learned and future needs', *Atmospheric Chemistry and Physics* **15**(14), 8217–8299.

Gaspari, L., Chang, S.-S., Santella, R. M., Garte, S., Pedotti, P. & Taioli, E. (2003), 'Polycyclic aromatic hydrocarbon-DNA adducts in human sperm as a marker of DNA damage and infertility', *Mutation Research/Genetic Toxicology and Environmental Mutagenesis* **535**(2), 155 – 160.

Ghigo, G., Causà, M., Maranzana, A. & Tonachini, G. (2006), 'Aromatic hydrocarbon nitration under tropospheric and combustion conditions. a theoretical mechanistic study', *The Journal of Physical Chemistry A* **110**(49), 13270–13282.

Giguère, P. A. & Maass, O. (1940), 'Vapour pressures and boiling points of binary mixtures of hydrogen peroxide and water', *Canadian Journal of Research* **18b**(7), 181–193.

Glowacki, D. R. & Pilling, M. J. (2010), 'Unimolecular reactions of peroxy radicals in atmospheric chemistry and combustion', *ChemPhysChem* **11**(18), 3836–3843.

Goldstein, A. H., Worton, D. R., Williams, B. J., Hering, S. V., Kreisberg, N. M., Panić, O. & Górecki, T. (2008), 'Thermal desorption comprehensive two-dimensional gas chromatography for in-situ measurements of organic aerosols', *Journal of Chromatography A* **1186**(1–2), 340 – 347. Trends and Developments in Gas Chromatography.

Gomez, M. E., Lin, Y., Guo, S. & Zhang, R. (2015), 'Heterogeneous chemistry of glyoxal on acidic solutions. an oligomerization pathway for secondary organic aerosol formation', *The Journal of Physical Chemistry A* **119**(19), 4457–4463.

Hallquist, M., Wenger, J. C., Baltensperger, U., Rudich, Y., Simpson, D., Claeys, M., Dommen, J., Donahue, N. M., George, C., Goldstein, A. H., Hamilton, J. F., Herrmann, H., Hoffmann, T., Iinuma, Y., Jang, M., Jenkin, M. E., Jimenez, J. L., Kiendler-Scharr, A., Maenhaut, W., McFiggans, G., Mentel, T. F., Monod, A., Prévôt, A. S. H., Seinfeld, J. H., Surratt, J. D., Szmigielski, R. & Wildt, J. (2009), 'The formation, properties and impact of secondary organic aerosol: current and emerging issues', *Atmospheric Chemistry and Physics* **9**(14), 5155–5236.

Heaton, K. J., Dreyfus, M. A., Wang, S., & Johnston*, M. V. (2007), 'Oligomers in the early stage of biogenic secondary organic aerosol formation and growth', *Environmental Science & Technology* **41**(17), 6129–6136.

Hildemann, L. M., Mazurek, M. A., Cass, G. R. & Simoneit, B. R. T. (1991), 'Quantitative characterization of urban sources of organic aerosol by high-resolution gas chromatography', *Environmental Science & Technology* **25**(7), 1311–1325.

Hyttinen, N., Knap, H. C., Rissanen, M. P., Jørgensen, S., Kjaergaard, H. G. & Kurtén, T. (2016), 'Unimolecular HO$_2$ loss from peroxy radicals formed in autoxidation is unlikely under atmospheric conditions', *The Journal of Physical Chemistry A* **120**(20), 3588–3595.

Hyttinen, N., Kupiainen-Määttä, O., Rissanen, M. P., Muuronen, M., Ehn, M. & Kurtén, T. (2015), 'Modeling the charging of highly oxidized cyclohexene ozonolysis products using nitrate-based chemical ionization', *The Journal of Physical Chemistry A* **119**(24), 6339–6345.

IARC (1983), 'Polynuclear aromatic compounds, part 1, chemical, environmental and experimental data.', *IARC Monogr Eval Carcinog Risk Chem Hum* **32**, 1–453.

Jacobson, M. Z. (2001), 'Strong radiative heating due to the mixing state of black carbon in atmospheric aerosols', *Nature* **409**(6821), 695–697.

Jokinen, T., Sipilä, M., Junninen, H., Ehn, M., Lönn, G., Hakala, J., Petäjä, T., Mauldin III, R. L., Kulmala, M. & Worsnop, D. R. (2012), 'Atmospheric sulphuric acid and neutral cluster measurements using CI-APi-TOF', *Atmospheric Chemistry and Physics* **12**(9), 4117–4125.

Junninen, H. (2014), 'Data cycle in atmospheric physics : From detected millivolts to understanding the atmosphere', *Report series in aerosol science* **145**.

Kalberer, M., Paulsen, D., Sax, M., Steinbacher, M., Dommen, J., Prevot, A. S. H., Fisseha, R., Weingartner, E., Frankevich, V., Zenobi, R. & Baltensperger, U. (2004), 'Identification of polymers as major components of atmospheric organic aerosols', *Science* **303**(5664), 1659–1662.

Kanakidou, M., Seinfeld, J. H., Pandis, S. N., Barnes, I., Dentener, F. J., Facchini, M. C., Van Dingenen, R., Ervens, B., Nenes, A., Nielsen, C. J., Swietlicki, E., Putaud, J. P., Balkanski, Y., Fuzzi, S., Horth, J., Moortgat, G. K., Winterhalter, R., Myhre, C. E. L., Tsigaridis, K., Vignati, E., Stephanou, E. G. & Wilson, J. (2005), 'Organic aerosol and global climate modelling: a review', *Atmospheric Chemistry and Physics* **5**(4), 1053–1123.

Kautzman, K. E., Surratt, J. D., Chan, M. N., Chan, A. W. H., Hersey, S. P., Chhabra, P. S., Dalleska, N. F., Wennberg, P. O., Flagan, R. C. & Seinfeld, J. H. (2010), 'Chemical composition of gas- and aerosol-phase products from the photooxidation of naphthalene', *The Journal of Physical Chemistry A* **114**(2), 913–934.

Keith, L. H. (2015), 'The source of U.S. EPA's sixteen PAH priority pollutants',
 Polycyclic Aromatic Compounds **35**(2-4), 147–160.

Keyte, I. J., Harrison, R. M. & Lammel, G. (2013), 'Chemical reactivity and long-
 range transport potential of polycyclic aromatic hydrocarbons - a review',
 Chem. Soc. Rev. **42**, 9333–9391.

Koch, R., Knispel, R., Elend, M., Siese, M. & Zetzsch, C. (2007), 'Consecutive re-
 actions of aromatic-OH adducts with NO, NO_2 and O_2: benzene, naphthalene,
 toluene, m- and p-xylene, hexamethylbenzene, phenol, m-cresol and aniline',
 Atmospheric Chemistry and Physics **7**(8), 2057–2071.

Kroll, J. H. & Seinfeld, J. H. (2008), 'Chemistry of secondary organic aerosol: For-
 mation and evolution of low-volatility organics in the atmosphere', *Atmospheric
 Environment* **42**(16), 3593 – 3624.

Kulmala, M. & Kerminen, V.-M. (2008), 'On the formation and growth of atmo-
 spheric nanoparticles', *Atmospheric Research* **90**(2), 132 – 150.

Kulmala, M., Vehkamäki, H., Petäjä, T., Maso, M. D., Lauri, A., Kerminen, V.-M.,
 Birmili, W. & McMurry, P. (2004), 'Formation and growth rates of ultrafine
 atmospheric particles: a review of observations', *Journal of Aerosol Science*
 35(2), 143 – 176.

Lambe, A. T., Ahern, A. T., Williams, L. R., Slowik, J. G., Wong, J. P. S., Abbatt,
 J. P. D., Brune, W. H., Ng, N. L., Wright, J. P., Croasdale, D. R., Worsnop,
 D. R., Davidovits, P. & Onasch, T. B. (2011), 'Characterization of aerosol pho-
 tooxidation flow reactors: heterogeneous oxidation, secondary organic aerosol
 formation and cloud condensation nuclei activity measurements', *Atmospheric
 Measurement Techniques* **4**(3), 445–461.

Lorenz, K. & Zellner, R. (1983), 'Kinetics of the reactions of OH-radicals with
 benzene, benzene-d6 and naphthalene', *Berichte der Bunsengesellschaft fur
 physikalische Chemie* **87**(8), 629–636.

McMurry, P. & Friedlander, S. (1979), 'New particle formation in the presence of
 an aerosol', *Atmospheric Environment (1967)* **13**(12), 1635 – 1651.

Miller, A. M., Yeung, L. Y., Kiep, A. C. & Elrod, M. J. (2004), 'Overall rate
 constant measurements of the reactions of alkene-derived hydroxyalkylperoxy
 radicals with nitric oxide', *Phys. Chem. Chem. Phys.* **6**, 3402–3407.

Nieminen, T., Lehtinen, K. E. J. & Kulmala, M. (2010), 'Sub-10 nm particle growth by vapor condensation – effects of vapor molecule size and particle thermal speed', *Atmospheric Chemistry and Physics* **10**(20), 9773–9779.

Nishino, N., Arey, J. & Atkinson, R. (2009), 'Yields of glyoxal and ring-cleavage co-products from the OH radical-initiated reactions of naphthalene and selected alkylnaphthalenes', *Environmental Science & Technology* **43**(22), 8554–8560.

Nishino, N., Arey, J. & Atkinson, R. (2012), '2-formylcinnamaldehyde formation yield from the OH radical-initiated reaction of naphthalene: Effect of NO_2 concentration', *Environmental Science & Technology* **46**(15), 8198–8204.

Nishino, N., Atkinson, R. & Arey, J. (2008), 'Formation of nitro products from the gas-phase OH radical-initiated reactions of toluene, naphthalene, and biphenyl: Effect of NO_2 concentration', *Environmental Science & Technology* **42**(24), 9203–9209.

NIST (2017), *NIST Chemistry WebBook*, National Institute of Standards and Technology.
URL: *http://webbook.nist.gov*

Orlando, J. J. & Tyndall, G. S. (2012), 'Laboratory studies of organic peroxy radical chemistry: an overview with emphasis on recent issues of atmospheric significance', *Chem. Soc. Rev.* **41**, 6294–6317.

Pankow, J. F. (1994), 'An absorption model of gas/particle partitioning of organic compounds in the atmosphere', *Atmospheric Environment* **28**(2), 185 – 188.

Perera, F., Hemminki, K., Jedrychowski, W., Whyatt, R., Campbell, U., Hsu, Y., Santella, R., Albertini, R. & O'Neill, J. P. (2002), 'In utero DNA damage from environmental pollution is associated with somatic gene mutation in newborns', *Cancer Epidemiology and Prevention Biomarkers* **11**(10), 1134–1137.

Pope, C. A. & Dockery, D. W. (2006), 'Health effects of fine particulate air pollution: Lines that connect', *Journal of the Air & Waste Management Association* **56**(6), 709–742.

Qu, X., Zhang, Q. & Wang, W. (2006), 'Mechanism for OH-initiated photooxidation of naphthalene in the presence of O_2 and NO_x: A DFT study', *Chemical Physics Letters* **429**(1–3), 77 – 85.

Ravindra, K., Sokhi, R. & Grieken, R. V. (2008), 'Atmospheric polycyclic aromatic hydrocarbons: Source attribution, emission factors and regulation', *Atmospheric Environment* **42**(13), 2895 – 2921.

Ravindra, Mittal, A. K. & Van Grieken, R. (2001), 'Health risk assessment of urban suspended particulate matter with special reference to polycyclic aromatic hydrocarbons: a review.', *Reviews on environmental health* **16**, 169–89.

Reisen, F. & Arey, J. (2005), 'Atmospheric reactions influence seasonal PAH and nitro-PAH concentrations in the Los Angeles Basin', *Environmental Science & Technology* **39**(1), 64–73.

Ricca, A. & Bauschlicher, Jr., C. W. (2000), 'The reactions of polycyclic aromatic hydrocarbons with OH', *Chemical Physics Letters* **328**, 396–402.

Robinson, A. L., Donahue, N. M., Shrivastava, M. K., Weitkamp, E. A., Sage, A. M., Grieshop, A. P., Lane, T. E., Pierce, J. R. & Pandis, S. N. (2007), 'Rethinking organic aerosols: Semivolatile emissions and photochemical aging', *Science* **315**(5816), 1259–1262.

Sakamoto, Y., Inomata, S. & Hirokawa, J. (2013), 'Oligomerization reaction of the criegee intermediate leads to secondary organic aerosol formation in ethylene ozonolysis', *The Journal of Physical Chemistry A* **117**(48), 12912–12921.

Sasaki, J., Aschmann, S. M., Kwok, E. S. C., Atkinson, R. & Arey, J. (1997), 'Products of the gas-phase OH and NO_3 radical-initiated reactions of naphthalene', *Environmental Science & Technology* **31**(11), 3173–3179.

Schauer, J. J., Kleeman, M. J., Cass, G. R. & Simoneit, B. R. T. (1999), 'Measurement of emissions from air pollution sources. 2. C_1 through C_{30} organic compounds from medium duty diesel trucks', *Environmental Science & Technology* **33**(10), 1578–1587.

Schauer, J. J., Kleeman, M. J., Cass, G. R. & Simoneit, B. R. T. (2001), 'Measurement of emissions from air pollution sources. 3. C_1–C_{29} organic compounds from fireplace combustion of wood', *Environmental Science & Technology* **35**(9), 1716–1728.

Schauer, J. J., Kleeman, M. J., Cass, G. R. & Simoneit, B. R. T. (2002), 'Measurement of emissions from air pollution sources. 5. C_1–C_{32} organic compounds from gasoline-powered motor vehicles', *Environmental Science & Technology* **36**(6), 1169–1180.

Seinfeld, J. H. & Pandis, S. N. (2006), *Atmospheric chemistry and physics: from air pollution to climate change*, John Wiley & Sons, Hoboken, New Jersey.

Shiraiwa, M., Ueda, K., Pozzer, A., Lammel, G., Kampf, C. J., Fushimi, A., Enami, S., Arangio, A. M., Fröhlich-Nowoisky, J., Fujitani, Y., Furuyama, A., Lakey, P.

S. J., Lelieveld, J., Lucas, K., Morino, Y., Pöschl, U., Takahama, S., Takami, A., Tong, H., Weber, B., Yoshino, A. & Sato, K. (2017), 'Aerosol health effects from molecular to global scales', *Environmental Science & Technology* **51**(23), 13545–13567.

Shiroudi, A., Deleuze, M. S. & Canneaux, S. (2014), 'Theoretical study of the oxidation mechanisms of naphthalene initiated by hydroxyl radicals: The OH-addition pathway', *The Journal of Physical Chemistry A* **118**(26), 4593–4610.

Silva, R. A., West, J. J., Zhang, Y., Anenberg, S. C., Lamarque, J.-F., Shindell, D. T., Collins, W. J., Dalsoren, S., Faluvegi, G., Folberth, G., Horowitz, L. W., Nagashima, T., Naik, V., Rumbold, S., Skeie, R., Sudo, K., Takemura, T., Bergmann, D., Cameron-Smith, P., Cionni, I., Doherty, R. M., Eyring, V., Josse, B., MacKenzie, I. A., Plummer, D., Righi, M., Stevenson, D. S., Strode, S., Szopa, S. & Zeng, G. (2013), 'Global premature mortality due to anthropogenic outdoor air pollution and the contribution of past climate change', *Environmental Research Letters* **8**(3), 034005.

Simonen, P., Saukko, E., Karjalainen, P., Timonen, H., Bloss, M., Aakko-Saksa, P., Rönkkö, T., Keskinen, J. & Dal Maso, M. (2016), 'A new oxidation flow reactor for measuring secondary aerosol formation of rapidly changing emission sources', *Atmospheric Measurement Techniques Discussions* **2016**, 1–27.

Stocker, F., Qin, D., Plattner, G.-K., Tignor, M., Allen, S., Boshung, A., Nauels, A., Xia, Y., Bex, V. & (eds.), P. M. (2013), *IPCC, 2013: Climate Change 2013: The Physical Science Basis. Contribution of Working Group I to the Fifth Assessment Report of the Intergovernmental Panel on Climate Change.*, Cambridge University Press.

Tsigaridis, K., Daskalakis, N., Kanakidou, M., Adams, P. J., Artaxo, P., Bahadur, R., Balkanski, Y., Bauer, S. E., Bellouin, N., Benedetti, A., Bergman, T., Berntsen, T. K., Beukes, J. P., Bian, H., Carslaw, K. S., Chin, M., Curci, G., Diehl, T., Easter, R. C., Ghan, S. J., Gong, S. L., Hodzic, A., Hoyle, C. R., Iversen, T., Jathar, S., Jimenez, J. L., Kaiser, J. W., Kirkevåg, A., Koch, D., Kokkola, H., Lee, Y. H., Lin, G., Liu, X., Luo, G., Ma, X., Mann, G. W., Mihalopoulos, N., Morcrette, J.-J., Müller, J.-F., Myhre, G., Myriokefalitakis, S., Ng, N. L., O'Donnell, D., Penner, J. E., Pozzoli, L., Pringle, K. J., Russell, L. M., Schulz, M., Sciare, J., Seland, Ø., Shindell, D. T., Sillman, S., Skeie, R. B., Spracklen, D., Stavrakou, T., Steenrod, S. D., Takemura, T., Tiitta, P., Tilmes, S., Tost, H., van Noije, T., van Zyl, P. G., von Salzen, K., Yu, F., Wang, Z., Wang, Z., Zaveri, R. A., Zhang, H., Zhang, K., Zhang, Q. & Zhang,

X. (2014), 'The AeroCom evaluation and intercomparison of organic aerosol in global models', *Atmospheric Chemistry and Physics* **14**(19), 10845–10895.

Umbuzeiro, G. A., Franco, A., Martins, M. H., Kummrow, F., Carvalho, L., Schmeiser, H. H., Leykauf, J., Stiborova, M. & Claxton, L. D. (2008), 'Mutagenicity and DNA adduct formation of PAH, nitro-PAH, and oxy-PAH fractions of atmospheric particulate matter from são paulo, brazil', *Mutation Research/-Genetic Toxicology and Environmental Mutagenesis* **652**(1), 72 – 80.

Volkamer, R., Jimenez, J. L., San Martini, F., Dzepina, K., Zhang, Q., Salcedo, D., Molina, L. T., Worsnop, D. R. & Molina, M. J. (2006), 'Secondary organic aerosol formation from anthropogenic air pollution: Rapid and higher than expected', *Geophysical Research Letters* **33**(17). L17811.

Wang, L., Wu, R. & Xu, C. (2013), 'Atmospheric oxidation mechanism of benzene. fates of alkoxy radical intermediates and revised mechanism', *The Journal of Physical Chemistry A* **117**(51), 14163–14168.

Wise, S. A., Sander, L. C. & Schantz, M. M. (2015), 'Analytical methods for determination of polycyclic aromatic hydrocarbons (PAHs) – a historical perspective on the 16 U.S. EPA priority pollutant PAHs', *Polycyclic Aromatic Compounds* **35**(2-4), 187–247.

Zelenyuk, A., Imre, D., Beránek, J., Abramson, E., Wilson, J. & Shrivastava, M. (2012), 'Synergy between secondary organic aerosols and long-range transport of polycyclic aromatic hydrocarbons', *Environmental Science & Technology* **46**(22), 12459–12466.

Zhang, Y. & Tao, S. (2009), 'Global atmospheric emission inventory of polycyclic aromatic hydrocarbons (PAHs) for 2004', *Atmospheric Environment* **43**(4), 812 – 819.

Zhang, Z., Lin, L. & Wang, L. (2012), 'Atmospheric oxidation mechanism of naphthalene initiated by OH radical. a theoretical study', *Phys. Chem. Chem. Phys.* **14**, 2645–2650.